TROPICAL OROGRAPHIC RAINFALL REGIMES ACCORDING TO THE TROPICAL RAINFALL MEASURING MISSION

BY

KIMBERLY ANN REED

THESIS

Submitted in partial fulfillment of the requirements
for the degree of Master of Science in Atmospheric Sciences
in the Graduate College of the
University of Illinois at Urbana-Champaign, 2011

Urbana, Illinois

Adviser:

Assistant Professor Stephen W. Nesbitt

ABSTRACT

Observing precipitation in tropical regions of complex terrain is a challenging problem. While ground-based instrumentation including rain gauge networks and radar data offer some insights, the lack of spatially complete gauge networks and radar artifacts such as severe beam blockage lead to large errors in the precipitation retrievals. The goals of this study are to understand what atmospheric variables and parameters influence tropical orographic precipitation and how these variables and parameters govern the precipitation intensity and patterns.

Twelve years (1998-2009) of data are used to determine which dynamic and thermodynamic variables and derived parameters interact to influence precipitation development and mode in multiple regions with varying orographic characteristics. NASA Modern Era Retrospective-Analysis for Research and Applications (MERRA) data over the tropical Andes, Hawaii, Eastern Himalayas, Sierra Madre Occidental, and Western Ghats are used to evaluate thirteen variables and parameters including convective available potential energy, convective inhibition, lifting condensation level, level of free convection, 700 hPa specific humidity, total precipitable water, 1000-700 hPa layer relative humidity, 700-300 hPa layer relative humidity, cross-barrier flow, mean virtual potential temperature, lapse rate of the mean virtual potential temperature, Brunt-Väisälä Frequency, and the moist Froude number. The variables and parameters are then organized into regimes specific to each individual region of complex terrain.

The Tropical Rainfall Measuring Mission (TRMM) precipitation radar (PR) 2A25v6 data is used to determine the vertical and horizontal structure and propagation of the precipitation systems as well as precipitation frequency and intensity.

The resulting regimes defined by the variables and parameters are compared to the TRMM PR data to examine how changes in the controlling atmospheric conditions impact the mode, propagation, and structure of the precipitation systems. Results indicate multiple variables and parameters have strong controls on regional orographic precipitation. Sounding and stability parameters tend to control precipitation patterns and locations while moisture variables tend to influence both frequency and intensity of the precipitation. On a multi-regional scale, moisture variables including 1000-700 hPa and 700-300 hPa layer relative humidities as well as 700 hPa specific humidity exhibit strong relationships with precipitation rate and frequency, and demonstrate the greatest universal applicability.

For my best friend and loving husband Justin and our family, Copper, Otis and Puma.

For my supportive and loving Mom and Dad.

For my caring brother and sister-in-law, Curtiss and Laura.

For my incredibly knowledgeable and encouraging grandparents,
Mr. & Mrs. Graydon and Donna Dill.

ACKNOWLEDGEMENTS

All of the hard work this thesis represents would not have been possible without the tremendous support from all of the great people I am blessed to have in my life. I am truly grateful to all of these people, and I know that I would not have been successful without all of the encouraging thoughts and love I have been surrounded with throughout the years.

My husband, best friend, and love of my life, Justin, has been there to help pick me up when I fall or get discouraged, and there have been a lot of those nights! He is always there to lend support, and remind me that I am very capable doing what is necessary to reach my goals. I thank him for the sacrifices he has made, so that I may strive to reach my goals.

My mom, Linda, has always been the stable rock in my life. I can't even imagine the possibility of reaching my goals without her by my side. Day or night, she is always there to lend an ear to listen, share her opinion, and give free hugs! I would have never made it this far without her.

I credit my dad, Randy, with showing me that life can change in a moment's notice, and to always be thankful for what you have because you never know what tomorrow will bring. I am incredibly thankful that he is around to share this major accomplishment with me.

I appreciated everything my brother and sister-in-law, Curtiss and Laura, have done for me. I would not have made it through undergrad without your continuous love and support.

My grandparents, Donna and the late Graydon Dill, are the inspiration I reflect on on a daily basis. They taught me the importance of education and success. They are the reason I am getting ready to start my Ph.D., and they were the reason I decided to go to graduate school in the first place. I could never have dreamed of goals this big without all of your encouragement, support, and help with my math homework! I am glad to be sharing this occasion with my Grandma, and I know my Grandpa is looking down from heaven and watching over me proudly.

I want to thank my tremendous advisor, Steve Nesbitt and his family. Without Steve's help and patients, I would have never made it this far! He is hands down, the best advisor I could have ever hoped for. His calm, laid back nature offsets my stressed out personality well, and his knowledge base is incredible. I also want to thank his family for being an inspiration to our family, and showing us that even with a crazy schedule, pets and kids are still possible!

Last, I want to thank a few members of my research group including Wendi, Dan, Kirstin, and Nicki as well as my friends in the Atmospheric Sciences Department. Your knowledge and previous experiences have been very helpful in reaching this goal.

This work has been funded by the NASA New Investigator Program as well as the NASA Earth System Science Fellowship.

TABLE OF CONTENTS

CHAPTER 1

INTRODUCTION AND LITERATURE REVIEW

1.1 – Introduction

Retrieving accurate precipitation measurements in regions of complex terrain is an arduous task. The complicated characteristics of mountainous regions lead to large errors in ground-based and space-based observations of precipitation. While rain gauge networks and ground-based radar data offer relatively low-error precipitation retrievals in homogenous terrain regions, problems including the lack of spatially complete rain gauge and radar networks, highly inhomogeneous spatial patterns of precipitation, and radar artifacts such as severe beam blockage lead to significantly larger rainfall rate retrieval errors in regions of complex terrain. These large errors in observed precipitation measurements are translated into amplified problems when used in hydrometeorological prediction, which can have a direct impact on a variety of issues ranging from predicting flash flooding to assessing the implications of natural and anthropogenic climate variability change. Due to the potential for significant societal and climate impacts, understanding the controlling atmospheric conditions underlying tropical orographic precipitation is a necessary step in reducing errors in real-time precipitation retrievals, and in turn improving quantitative precipitation estimation and hydrometeorological prediction.

1.2 – Observational Studies

Very limited observational work has been done on orographic precipitation in the Tropics. A study of Hawaii by Smolarkiewicz et al. (1988) during the Joint Hawaiian Warm Rain Project focused on the forcing mechanism behind band clouds that form just off shore on the northeast side of the Big Island of Hawaii. The study analyzed the band cloud presence and movement in relation to the Froude number, which is a function of the mean upstream wind, static stability, and mountain height. The analysis revealed that the band cloud formed on a quasi-stationary low-level convergence zone, and the main determinant of the strength and location of the convergence zone was the Froude number. When the Froude number was low, the band cloud was very pronounced, but as the Froude number increased, the band cloud was no longer present and was instead replaced with clouds and precipitation on the windward slope of the island.

1.3 – Modeling Studies

From a numerical modeling standpoint, orographic precipitation has been thoroughly studied in the mid-latitudes, but to a lesser degree in the Tropics. A study by Chen and Lin (2005) used idealized simulations consisting of a two-dimensional mountain ridge and conditionally unstable flow to investigate the impacts the unsaturated moist Froude number (F_w) and convective available potential energy (CAPE) have on the propagation and types of cloud precipitation systems. The results consisted of four basic flow regimes determined by the

relationship between F_w and CAPE. The study showed that by analyzing a combination of the parameters, upstream, downstream, or stationary movement could be determined as well as whether the system would have convective or stratiform precipitation.

A more recent modeling study by Miglietta and Rotunno (2009) utilized a three-dimensional domain to understand the impacts of the environmental wind speed on the propagation of orographic precipitation. The analysis showed that for weaker environmental wind speeds, evaporative cooling from precipitation contributed to a cold pool that resulted in cold air outflow, which became the main driver of cell propagation and redevelopment. Because the newly developed cells formed on the edge of the rapidly propagating outflow, the majority of the precipitation was located away from the ridge. For higher environmental wind speeds, the precipitation system was already propagating at a speed that was not conducive to strong cold pool development, and therefore more precipitation fell over the ridge.

1.4 – Motivation

The observational and modeling studies have provided a number of varying analyses and arguments regarding the dynamics of orographic precipitation. However, there exists a lack of global observational studies of the factors controlling the spatial distribution and intensity of orographic precipitation. While the observational findings in Hawaii are a good starting point, Hawaii is known for

having 3-D volcano-like mountains being completely surrounded by water. Features such as the trade wind inversion likely play a large role in precipitation characteristics, which may not be found in other regions of complex terrain in the Tropics. The idealized mountains found in most modeling studies of orographic precipitation in tropical conditions are made up of a single ridge perpendicular to the flow. A simple ridge system is not characteristic of the mountain ranges found around the world, which may consist of a single plateau, a series of sharp peaks and valleys, or multiple ridges offset by vast canyons.

Due to these limitations in past work, this study will focus on trying to determine what environmental characteristics modulate the spatial distribution and intensity of orographic precipitation in multiple tropical regions with varying complex terrain characteristics.

CHAPTER 2

DATA AND METHODOLOGY

2.1 – Reanalysis Data

NASA Modern Era Retrospective-Analysis for Research and Applications (MERRA) is used in this study to analyze the dynamic and thermodynamic variables and parameters. MERRA is a modern satellite era (1979-present) reanalysis produced by NASA's Global Modeling and Assimilation Office and assimilates traditional and satellite observations from multiple platforms. MERRA was produced at a horizontal resolution of 1/2° latitude x 2/3° longitude using the Goddard Earth Observing System Data Assimilation System Version 5 (GEOS-5) (Rienecker et al. 2011). GEOS-5 contained 72 vertical levels extending from the surface to 0.01 hPa and utilized Incremental Analysis Updates (IAU) coupled with the traditional reanalysis observations of temperature, wind speed, and pressure and NASA's Earth Observing System (EOS) satellite observations to nudge the model states closer to the observed state. This study utilizes two MERRA products. The first product is the 3-hourly instantaneous assimilated state on pressure EOS core system MAI3CPASM product. The data has a 1.25° latitude x 1.25° longitude horizontal resolution and contains 42 interpolated vertical pressure levels ranging from 1000 hPa to 0.1 hPa. Variables extracted from the MAI3CPASM product include geopotential height, surface geopotential, surface pressure, specific humidity, relative humidity, temperature, eastward wind component, and

northward wind component. The second product used in this study is the hourly instantaneous MAI1NXINT product, which has a horizontal resolution of 1/2° latitude by 2/3° longitude and contains vertically integrated parameters including total column water vapor, which was used for this study.

2.2 – Satellite Data

The satellite data used to evaluate precipitation characteristics in this study are from the Tropical Rainfall Measuring Mission (TRMM). TRMM is an ongoing joint effort between NASA and the Japan Aerospace Exploration Agency (JAXA) with the purpose of providing a platform to monitor and investigate tropical rainfall. TRMM has an onboard suite of instruments including the precipitation radar (PR), microwave imager (TMI), visible and infrared scanner (VIRS), cloud and earth radiant energy sensor (CERES), and lightning imaging sensor (LIS) (Kummerow et al. 1998). This study will focus on the precipitation radar for rainfall retrievals. TRMM was launched on 27 November 1997 and became fully operational on 8 December 1997. TRMM initially orbited at an altitude of 350 km AGL. On 24 August 2001 in an effort to extend the lifetime of the satellite, the TRMM satellite boost was completed with a final orbiting altitude of 402.5 km AGL.

The TRMM PR is the first spaceborne radar designed specifically for precipitation retrievals and remains the current standard in spaceborne rainfall measurements in the Tropics. TRMM completes approximately 16 orbits per day with each orbit taking 92.5 minutes to complete. The PR has a horizontal resolution

of 5 km and a vertical resolution of 250 m at nadir. Three-dimensional rainfall measurements are taken using an electronically scanning phased array antenna operating at 13.8 GHz.

TRMM PR offers multiple raw and algorithm corrected data sets for use in precipitation analyses (Iguchi et al. 2000). The TRMM PR 2A25 version 6 (2A25v6) Rainfall Rate and Profile Product is a Level 2 product that encompasses PR attenuation corrected reflectivities. The TRMM PR 2A25v6 data will be used to analyze orographic precipitation characteristics for this study.

2.3 – Regions of Interest

This study will focus on wet season precipitation analyses in five regions with drastically varying atmospheric and terrain characteristics. The selected regions are chosen based on their locations within the Tropics and their diverse range of geographic and meteorological characteristics. Each region consists of a 10° x 10° area which encompasses the complex terrain of interest. The regions include the tropical Andes, Hawaii, the Eastern Himalayas, the Sierra Madre Occidental, and the Western Ghats as seen in Figure 1.

The tropical Andes region is located at 0°N to 10°N and 70°W to 80°W in northwestern South America. The range has an average mountain height of 3000 m and is characterized by tall peaks and large valleys. Peak wet season for the tropical Andes occurs from 1 December through 28 February.

The region encompassing Hawaii is located at 14°N to 24°N and 152°W to 162°W in the North Pacific Ocean and includes the island of Hawaii surrounded entirely by water. The study will focus on the volcanic mountain range located on the Big Island of Hawaii including the peaks of Mauna Kea, Mauna Loa, and Kīlauea, which have an average mountain height of 3000 m. Hawaii's wet season runs from 1 December through 28 February.

The Eastern Himalayas region contains the tallest region of complex terrain this study will focus on with an average mountain height of 5000 m. The Himalayas are located in southern Asia at 22°N to 32°N and 85°E to 95°E and serve as the divider between the Indian subcontinent and the Tibetan Plateau. Peak wet season for the Himalayas occurs from 1 May to 30 September.

The Sierra Madre Occidental (SMO) region is located at 20°N to 30°N and 100°W to 110°W along the western coast of Mexico. The complex terrain is characterized by steep ridges and vast canyons and has an average mountain height of 2500 m. The peak wet period occurs during the monsoon season of 15 June through 30 September.

The last region of focus for this study includes the Western Ghats located at 10°N to 20°N and 70°E to 80°E on the west coast of India. The Western Ghats serve as the divider between the coastal plain and the Deccan Plateau and have an average mountain height of 1500 m. The wet season for the area occurs 1 May through 30 September.

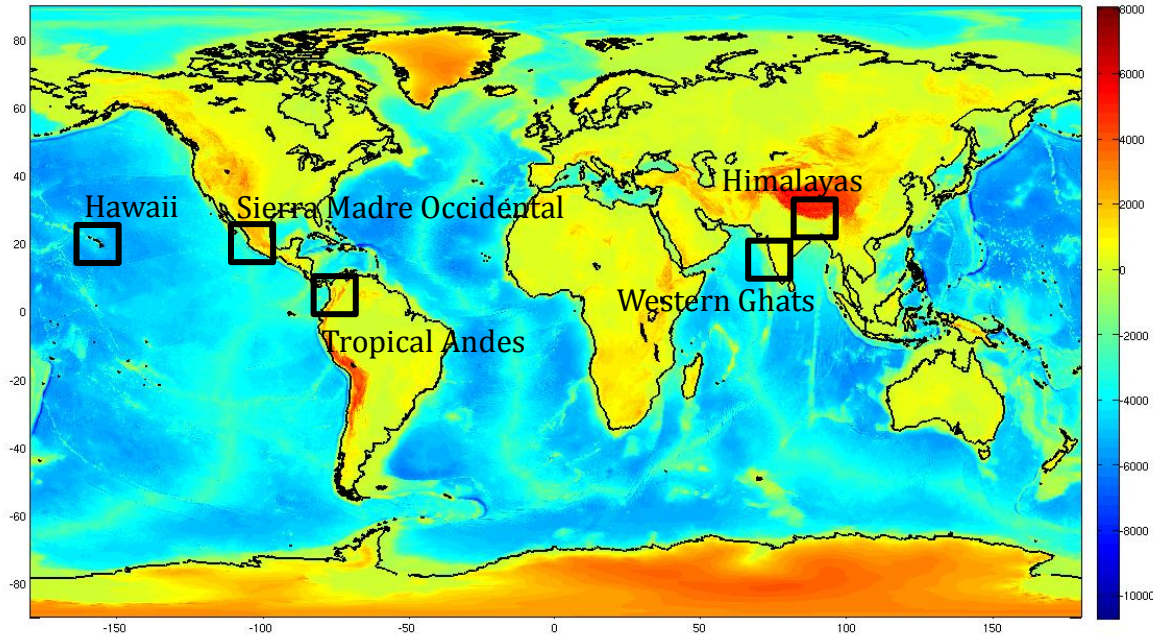

Figure 1. Topographic map of the world with elevations colored in meters. Black boxes indicate the 10° x 10° regions of interest.

2.4 – Variables and Parameters

This analysis will focus on thirteen variables and parameters to determine how each atmospheric control parameter affects orographic precipitation characteristics in the regions of interest. The variables and parameters are sorted into three categories including sounding parameters, moisture variables, and stability parameters.

Several sounding parameters have been chosen for analysis in this study. These include convective available potential energy ($CAPE$), convective inhibition (CIN), lifting condensation level (LCL), and level of free convection (LFC) and are

calculated using MERRA variables. CAPE is the amount of energy available for parcel convection and is calculated using the following (Emanuel, 1994):

$$CAPE_i = \int_{p_n}^{p_i} R_d\left(T_{\rho p} - T_{\rho a}\right) d \ln p$$

The amount of energy needed to vertically lift a parcel to the parcel's level of free convection is defined as CIN and is calculated using the following (Emanuel, 1994):

$$NA_i = -\int_{p_f}^{p_i} R_d \left(T_{\rho p} - T_{\rho a}\right) d \ln p$$

The point at which a moist air parcel lifted dry-adiabatically becomes saturated is the LCL. The LCL is calculated using the following (Emanuel, 1994):

$$z^* - z = \frac{c_{pd}}{g} \frac{1 + r\frac{c_{pv}}{c_{pd}}}{1 + r} (T - T^*)$$

The height at which the parcel becomes warmer than the environment is the LFC, which is calculated based on ambient air temperature and parcel temperature.

The moisture parameters chosen for analysis in this study represent multiple indices at relevant levels throughout the atmosphere. The moisture controls include specific humidity, precipitable water, and relative humidity. Specific humidity at the 700 hPa level (QV_{700}) is used due to the temperature independence of the parameter. Total precipitable water (PW) is useful as an indicator of boundary layer moisture. Relative humidity within the 1000 hPa to 700 hPa layer ($RH_{1000-700}$) is evaluated as an indicator of low-level moisture and relative

humidity within the 700 hPa to 300 hPa layer ($RH_{700-300}$) as an indicator of mid-level moisture.

The last category of parameters is calculated using MERRA data and encompasses the stability parameters of cross-barrier flow (u^*), mean virtual potential temperature ($\bar{\theta}_v$), lapse rate of the mean virtual potential temperature $\left(\frac{d\bar{\theta}_v}{dz}\right)$, Brunt-Väisälä Frequency (N_w), and moist Froude number (F_w). Cross-barrier flow is flow that is perpendicular to the mountain range and is used to analyze upslope flow effects on orographic precipitation. Cross-barrier flow is calculated by rotating the mean winds into a terrain-perpendicular frame of reference. The angle of rotation is different for each region of complex terrain as seen in Table 1. Positive values of cross barrier flow are defined to blow in the direction of the climatological prevailing wind direction.

The mean virtual potential temperature is defined as the potential temperature dry air would need to be in order to have the same density as moist air. For this study $\bar{\theta}_v$ is calculated for the lowest 250 hPa using the following (Emanuel, 1994):

$$\bar{\theta}_v = avg\left[T_v\left(\frac{1000}{p}\right)^{R_d/c_{pd}}\right]$$

where T_v is the virtual temperature, p is the pressure level of interest, R_d is the gas constant for dry air, and c_{pd} is the heat capacity of dry air at constant pressure. The lapse rate of the mean virtual potential temperature is the change of the mean virtual potential temperature with height and is calculated over the lowest 250 hPa. The lapse rate is used to calculate the Brunt-Väisälä frequency, which is a parameter

for static stability analysis. The Brunt-Väisälä frequency is calculated using the following (Emanuel, 1994):

$$N_w = \sqrt{\frac{g}{\bar{\theta}_v}\frac{d\bar{\theta}_v}{dz}}$$

The Brunt-Väisälä frequency, cross-barrier flow, and mountain height are then used to calculate the moist Froude number using the following (Chen and Lin, 2005):

$$F_w = \frac{u^*}{N_w h}$$

where *h* is the average mountain height listed in Table 1. The moist Froude number is calculated to analyze mountain flow patterns such as blocking.

Region	Average Mountain Height	Angle of Rotation
Western Ghats	1500 m	20°
Eastern Himalayas	5000 m	90°
Tropical Andes	3000 m	0°
Sierra Madre Occidental	2500 m	35°
Hawaii	3000 m	45°

Table 1. Average mountain height and angle of rotation used to calculate cross-barrier flow and the moist Froude number for individual regions of complex terrain.

2.5 – Defining an Upstream Region

In order to evaluate orographic precipitation characteristics over and in the immediate vicinity of the complex terrain, we define so-called upstream regions in an attempt to analyze airmass dynamical and thermodynamical characteristics prior to these airmasses impinging on the terrain. Using the prevailing wind direction in the wet seasons determined from MERRA at the vertical levels defined below for each region, the upstream region is defined spatially in an attempt to be sufficiently far enough upstream from the terrain to not be influenced by the terrain itself. The level of the mean winds used to define the upstream regions for Hawaii and the Western Ghats is 925 hPa. Near-surface mean winds were chosen for these regions as flow is coming directly off an ocean and is not impeded by any land surfaces of higher elevation before reaching the complex terrain of interest. For the tropical Andes, eastern Himalayas, and Sierra Madre Occidental, 700 hPa mean winds are used to determine the upstream regions. Low-level winds are used for these regions, as upstream flow is traveling over land surfaces before reaching the complex terrain. Figure 2 shows topographic maps of each region of complex terrain overlain with the corresponding level of mean winds used to define the upstream region. The black boxes indicate the defined upstream regions for which variables and parameters are evaluated.

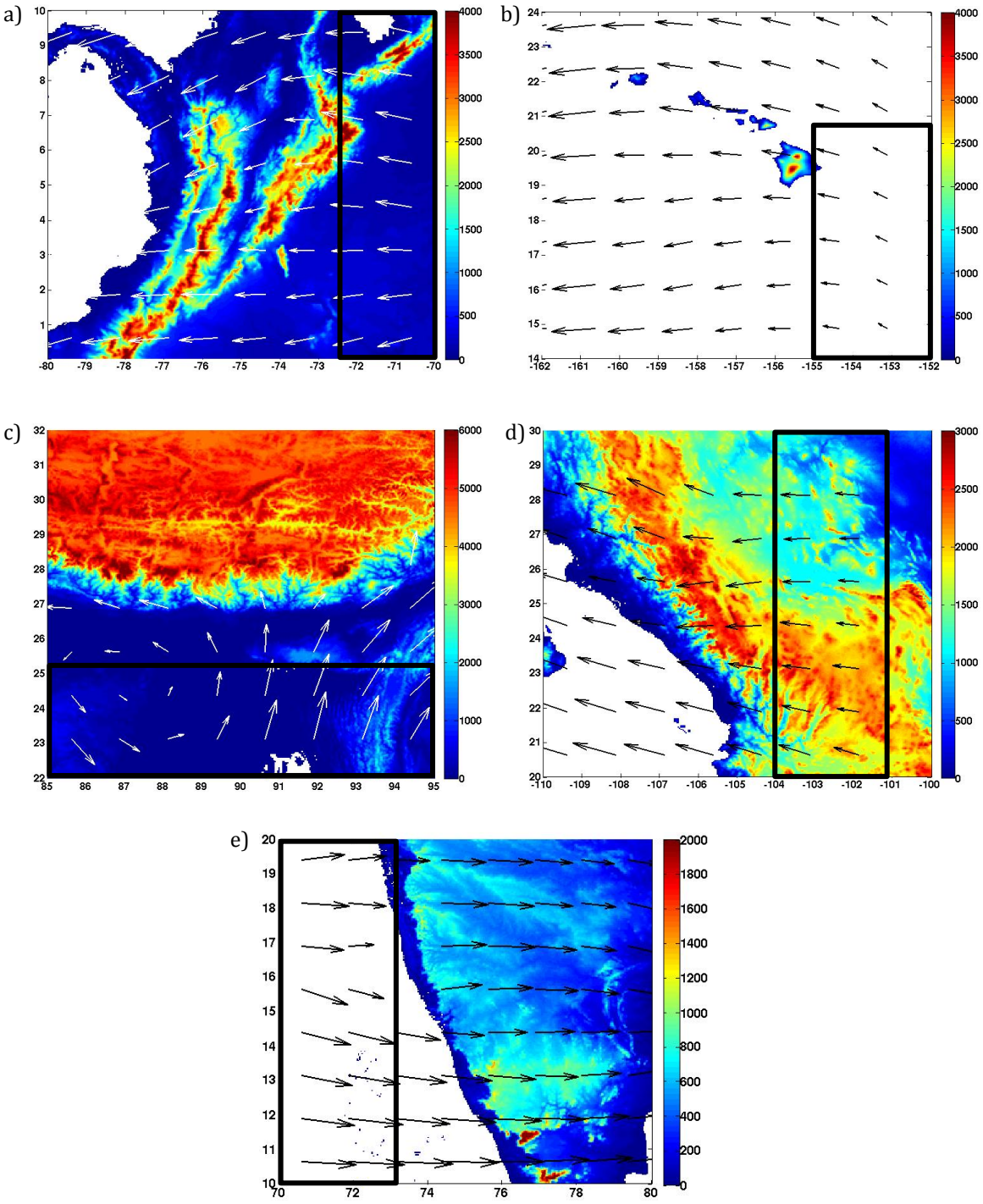

Figure 2. Elevation map of terrain in meters overlaid with wind flow used to determine upstream region. Black box indicates defined upstream region. (a) Tropical Andes, 700 hPa mean wind (b) Hawaii, 925 hPa mean wind (c) Eastern Himalayas, 700 hPa mean wind (d) Sierra Madre Occidental, 700 hPa mean wind (e) Western Ghats, 925 hPa mean wind.

2.6 – Data Subsetting

In order to make intercomparisons between multiple variables and parameters as well as relate the data to the TRMM PR products for analysis, each data set corresponding to a specific variable or parameter is first sorted by the variable value. For regional analyses, the variable value-sorted data sets are then subsetted into even thirds. For multi-regional analyses, the variable sorted data sets are evenly divided into twenty subsets subsetted by variable value. By subsetting the data into even bins, the need to set any artificial thresholds on the variables and parameters is eliminated.

2.7 – MERRA and TRMM PR Data Matching

The last step before precipitation analysis involves matching the subset variable and parameter MERRA data sets to the corresponding TRMM data sets. Due to the relatively infrequent sampling of the TRMM orbit, there is not a TRMM PR 2A25v6 observation for each MERRA data point. Composites are created of TRMM PR products, and when subsetted by variable, are associated with the closest 3 hour MERRA output time.

CHAPTER 3

RESULTS

Two main focus areas will be discussed in the results section. The individual regional precipitation analyses will be examined first to determine how the variables and parameters of interest uniquely impact each region of complex terrain. Following the individual analyses, the data will be combined into multi-regional precipitation analyses to examine the inter-regional variability of precipitation characteristics.

3.1 – Regional Analyses

To determine how the variables and parameters impact tropical orographic precipitation in regions with varying terrain characteristics, dynamic and thermodynamic variables and parameters will be analyzed separately for each region of interest.

Rain rate and rain frequency are used to evaluate precipitation characteristics in each region. Rain rate is a measure of the intensity of the precipitation falling over a given amount of time. For this study rain rate is defined in mm day^{-1}. Rain frequency indicates the number of occurrences precipitation is detected over a specified time frame. Composite plots of rain rate and rain frequency are used to analyze the precipitation relationships for each of the three subsets for each variable and parameter.

3.1.1 – Tropical Andes

Sounding parameters play a key role in determining the precipitation location in the tropical Andes. Figure 3 shows that for low CAPE situations, the highest rain frequencies are confined to the mountain peaks, while the highest rain rates are sporadically located along the peaks as well as over the ocean (Figs. 3a, 3d). As the CAPE increases, precipitation becomes more widespread and increases in frequency and rain rate (Figs. 3b, 3e). When the CAPE reaches a threshold value near 700 J kg^{-1}, the highest rain frequencies become collocated with areas of higher terrain (Figs. 3c, 3f). This may be a result of the unstable air allowing for continuous redevelopment of convection over the higher terrain.

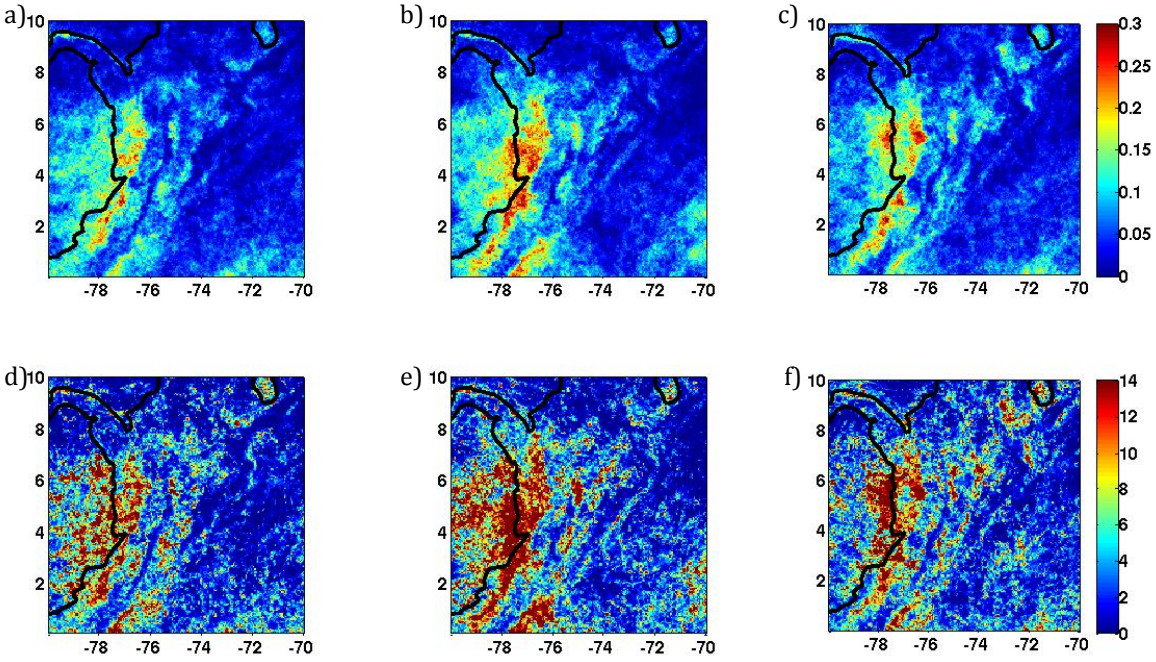

Figure 3. Tropical Andes TRMM PR 2A25v6 precipitation products for CAPE subsets. Top three panels are rain frequency and bottom three panels are rain rate in mm day^{-1}. CAPE values range from (a,d) 74.3 – 529.6 J kg^{-1} (0-33%), (b,e) 529.6 – 700.0 J kg^{-1} (33-66%), and (c,f) 700.0 – 1451.9 J kg^{-1} (66-100%).

Moisture variables are important in determining precipitation intensity in the tropical Andes. Analyses of 700 hPa to 300 hPa relative humidity show that, as more mid-level moisture becomes available, precipitation frequency increases significantly further inland (Fig. 4). The highest frequencies occur on the peaks closest to the coast, while the highest rain rates occur along the coast and slightly off shore (Figs. 4c, 4f).

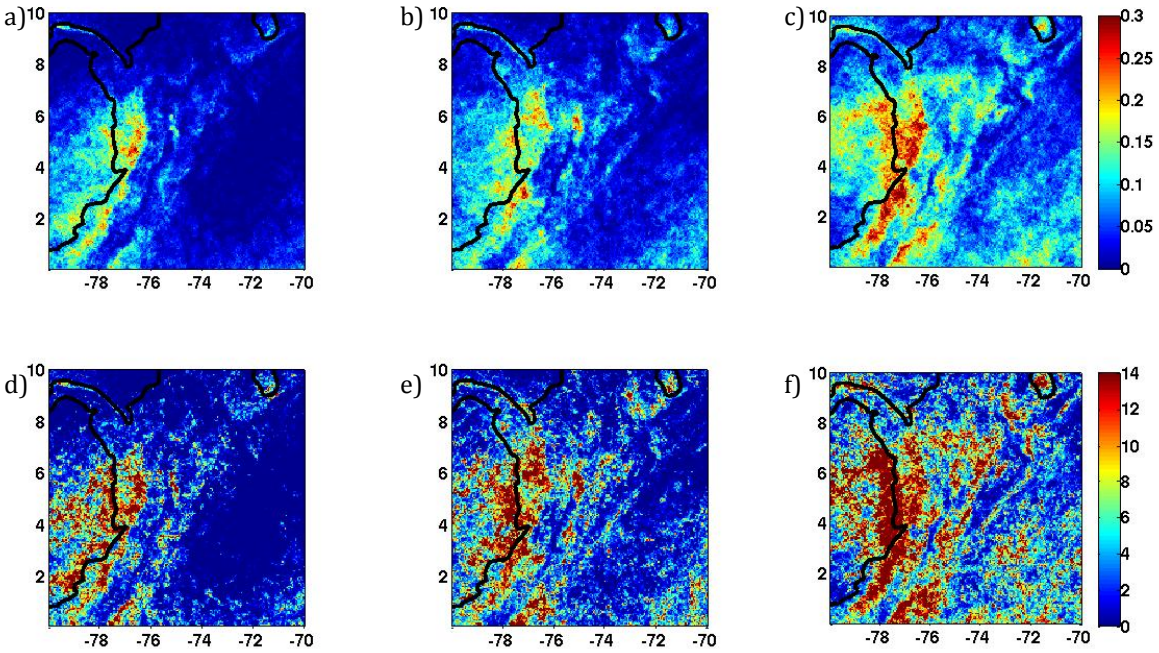

Figure 4. Tropical Andes TRMM PR 2A25v6 precipitation products for the 700-300 layer relative humidity subsets. Top three panels are rain frequency and bottom three panels are rain rate in mm day^{-1}. $RH_{700\text{-}300}$ values range from (a,d) 14.6 – 56.0% (0-33%), (b,e) 56.0 – 69.8% (33-66%), and (c,f) 69.8 – 94.2% (66-100%).

3.1.2 – Hawaii

The lapse rate of the mean virtual potential temperature has a large influence on precipitation frequency and rain rates on the Big Island of Hawaii. Low lapse rates in the low levels of the atmosphere lead to the highest rain rates and rain

frequencies for the island as seen in Figure 5. The increased intensity and frequency are likely due to the increased instability that accompanies the lower lapse rates. The instability allows the precipitation to ascend up the slope of the terrain with minimal external forcing.

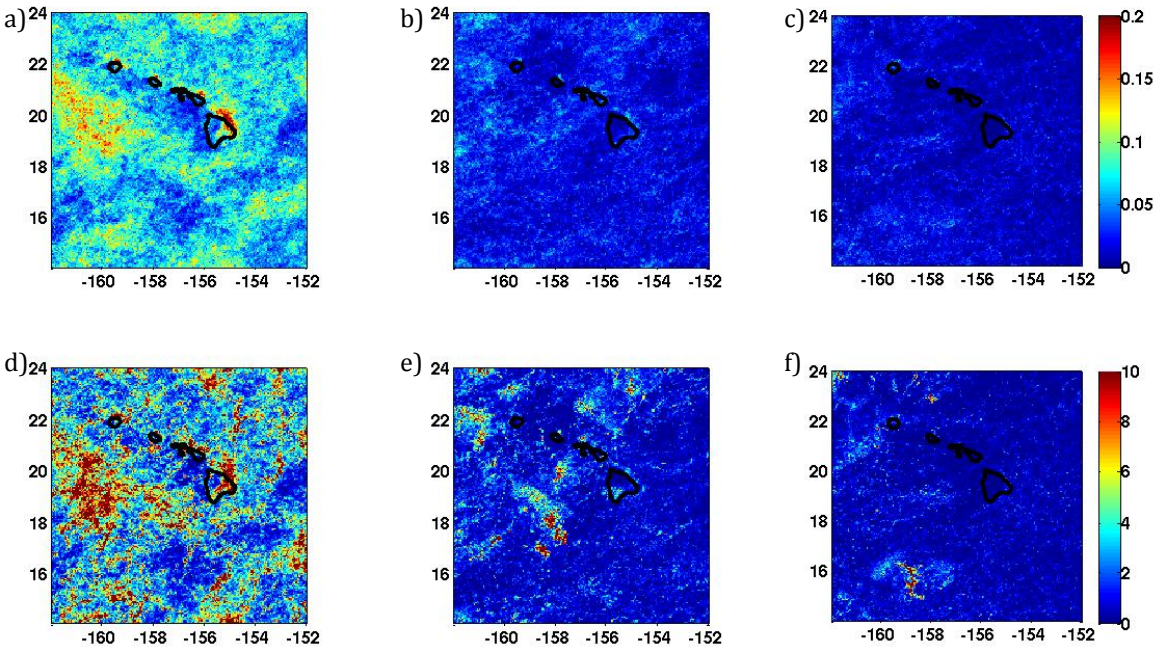

Figure 5. Hawaii TRMM PR 2A25v6 precipitation products for the lapse rate of the mean virtual potential temperature subsets. Top three panels are rain frequency and bottom three panels are rain rate in mm day^{-1}. Lapse rate values range from (a,d) 2.9 – 4.2 K m^{-1} (0-33%), (b,e) 4.2 – 4.9 K m^{-1} (33-66%), and (c,f) 4.9 – 6.6 K m^{-1} (66-100%).

The moist Froude number also plays a key role in orographic precipitation patterns and intensity on the Big Island of Hawaii. When the moist Froude number is low, both precipitation frequency and intensity are low (Figs. 6a, 6d). As the moist Froude number increases, precipitation begins to increase on the windward side of the terrain, but very little happens over the peaks (Figs. 6c, 6f). The lack of precipitation over the peaks may be the result of blocking which acts to redirect the

flow around the range and prevents precipitation from reaching the peaks (Yang and Chen 2008).

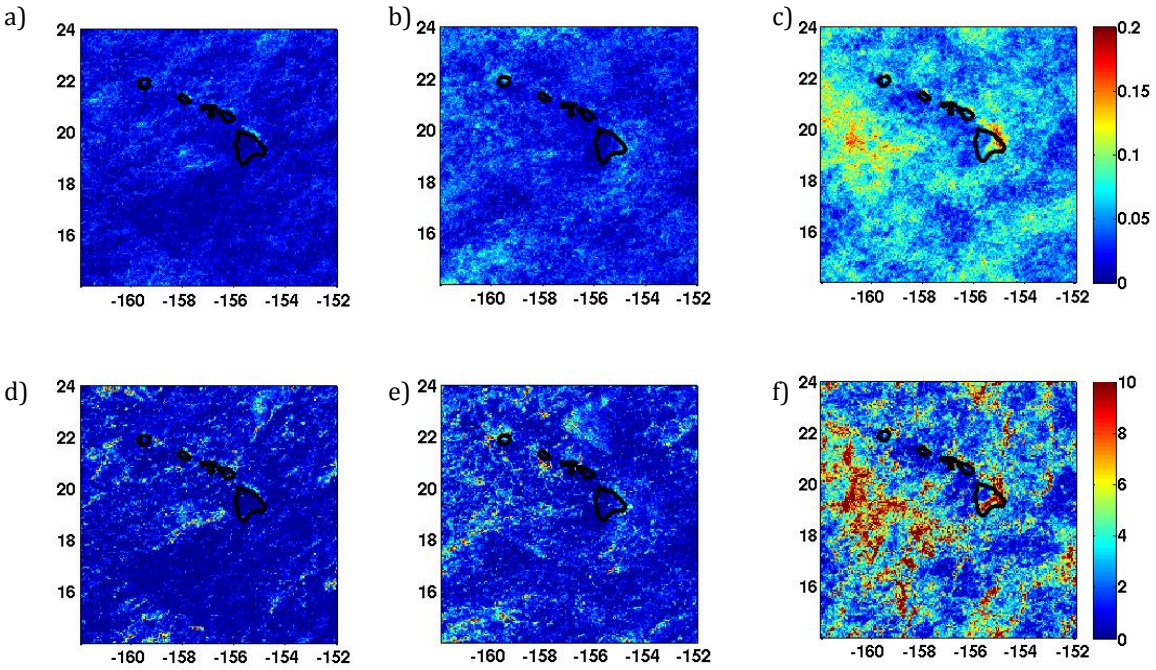

Figure 6. Hawaii TRMM PR 2A25v6 precipitation products for the moist Froude number subsets. Top three panels are rain frequency and bottom three panels are rain rate in mm day^{-1}. F_w values range from (a,d) -0.30 – 0.06 s^{-1} (0-33%), (b,e) 0.06 – 0.12 s^{-1} (33-66%), and (c,f) 0.12 – 0.44 s^{-1} (66-100%).

3.1.3 – Eastern Himalayas

Parcel forcing is a determining factor of precipitation location patterns in the in the Eastern Himalayas. Figure 7 shows the LFC precipitation products for the Eastern Himalayas. For low LFC heights, precipitation is widespread and found over both the peaks and lower terrain areas (Figs. 7a, 7d). As the LFC height increases, the precipitation pattern changes, and precipitation is confined mainly to the areas of higher terrain (Figs. 7c, 7f). An increase in LFC heights means the parcel likely needs more external forcing to reach the level where the parcel becomes positively

bouyant, and therefore the precipitation is confined to higher terrain where the orographic forcing is present.

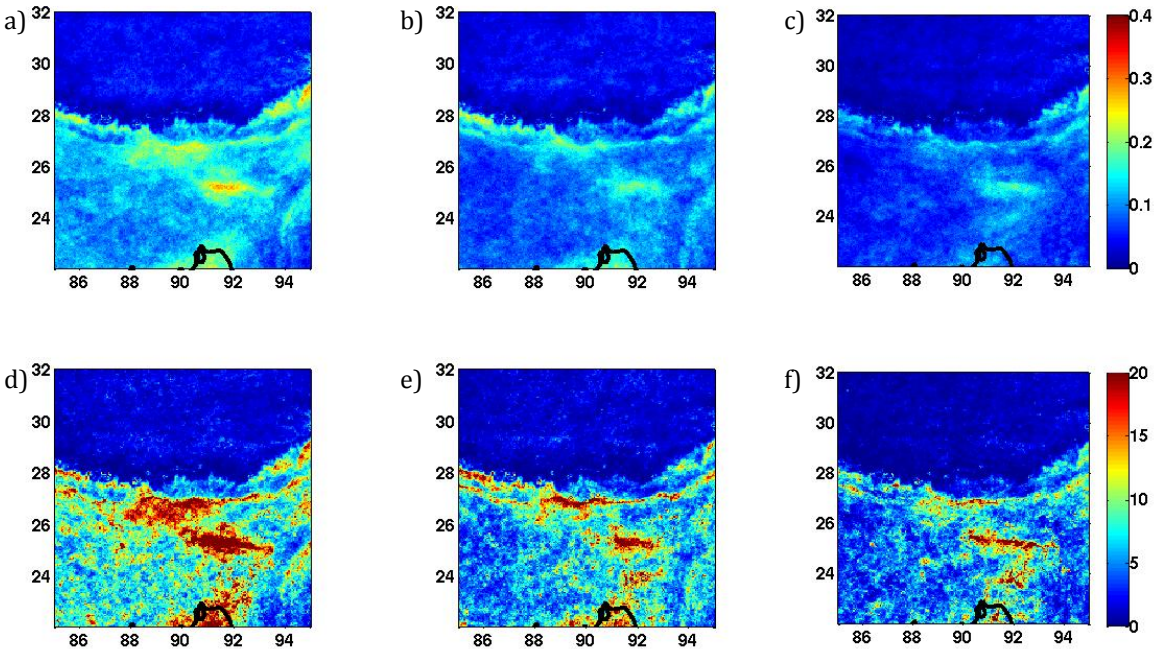

Figure 7. Eastern Himalayas TRMM PR 2A25v6 precipitation products for the level of free convection subsets. Top three panels are rain frequency and bottom three panels are rain rate in mm day^{-1}. LFC values range from (a,d) 763.2 – 1368.6 m (0-33%), (b,e) 1368.6 – 2616.9 m (33-66%), and (c,f) 2616.9 – 63719.0 m (66-100%).

The effects of the moist Froude number on precipitation frequency and rain rate in the Eastern Himalayas are similar to those found in Hawaii. For low moist Froude numbers, rain frequency and rain rate are kept to a minimum over the higher terrain and are found to be greater in areas of lower terrain as seen in Figure 8. As the moist Froude number increases, the mode of the frequency and intensity of the precipitation rapidly changes. With increasing moist Froude number, higher elevation regions have a sharp increase in rate and intensity, while lower elevation regions see a decrease (Figs. 8c, 8f). The drastic change in precipitation frequency

and rate demonstrates the ability of the moist Froude number to be used as an indicator of blocked flow. For low moist Froude numbers, flow over the higher terrain is blocked, so little precipitation falls over the windward slopes, but as the moist Froude number increases, flow is able to reach the higher terrain areas, which explains the large increase in rate and intensity over the slopes.

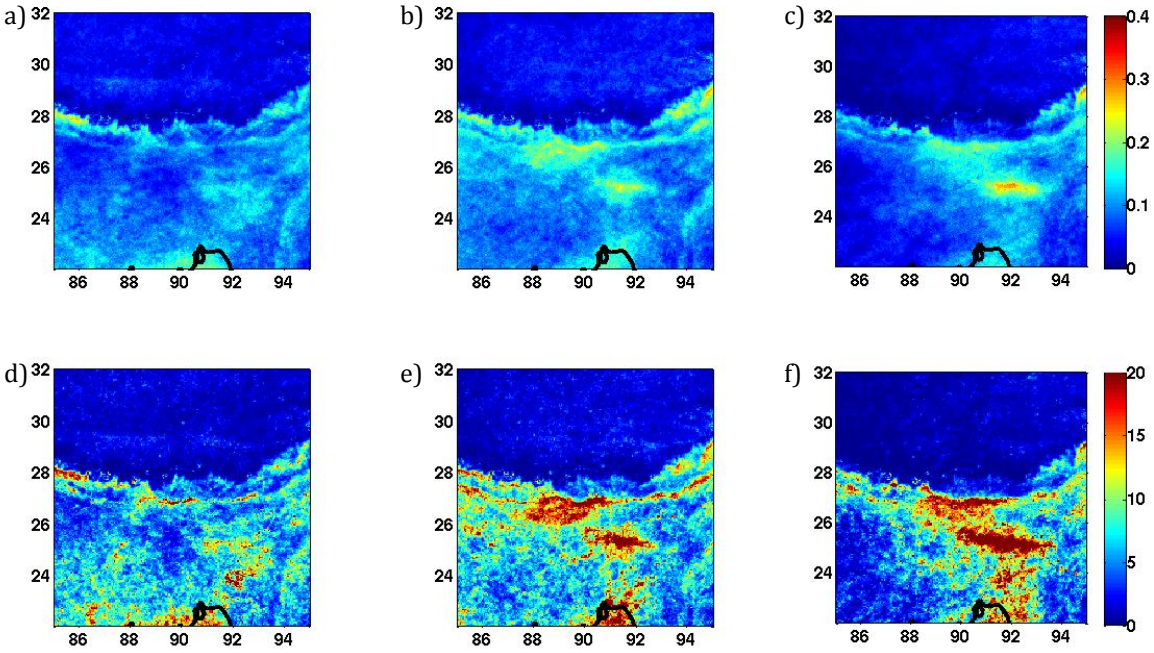

Figure 8. Eastern Himalayas TRMM PR 2A25v6 precipitation products for the moist Froude number subsets. Top three panels are rain frequency and bottom three panels are rain rate in mm day^{-1}. F_w values range from (a,d) -0.09 – 0.01 s^{-1} (0-33%), (b,e) 0.01 – 0.04 s^{-1} (33-66%), and (c,f) 0.04 – 0.12 s^{-1} (66-100%).

3.1.4 – Sierra Madre Occidental

Precipitation location patterns and frequency in the Sierra Madre Occidental are impacted greatly by sounding parameters. For low LCL heights, precipitation is frequent over a broad area that includes, but is not limited to the complex terrain (Figs. 9a, 9d). As the LCL height increases, the precipitation frequency decreases

over all regions (Figs. 9c, 9f). At the same time, the precipitation becomes confined to regions of higher terrain. The pattern and frequency changes are likely the result of an increased need for external forcing as the LCL height increases. Diurnal forcing likely becomes the external forcing mechanism and allows for precipitation to still occur over the peaks, but with decreased frequency (Nesbitt et al., 2008).

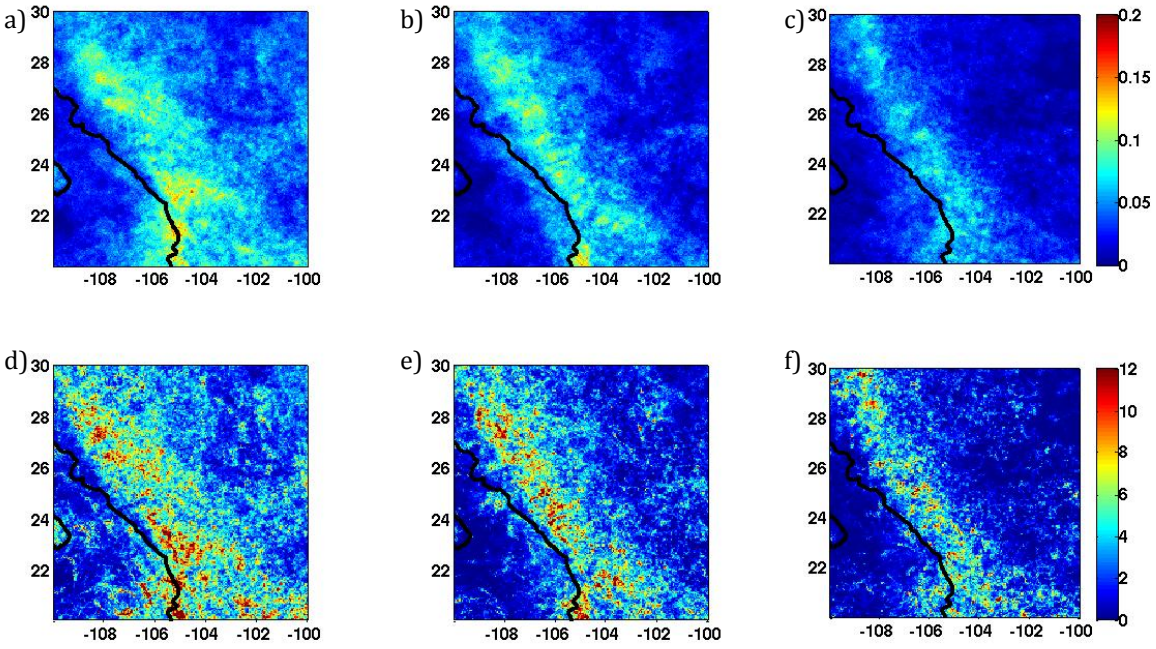

Figure 9. Sierra Madre Occidental TRMM PR 2A25v6 precipitation products for the LCL subsets. Top three panels are rain frequency and bottom three panels are rain rate in mm day^{-1}. LCL values range from (a,d) 711.1 – 1166.8 m (0-33%), (b,e) 1166.8 – 1444.5 m (33-66%), and (c,f) 1444.5 – 3331.3 m (66-100%).

The effects of moisture are important for precipitation intensity and frequency as well as overall precipitation location patterns over the Sierra Madre Occidental. Figure 10 indicates that total precipitable water is a controlling factor in orographic precipitation. For drier air, precipitation is confined mainly to the higher terrain areas, and frequencies and rain rates are low (Figs. 10a, 10d). As

more moisture becomes available, the precipitation becomes more widespread and the frequency and rain rate over the higher elevations increases (Figs. 10c, 10f). The rain rate off the coast also increases with increased moisture, which may be the result of diurnal mesoscale convective systems propagating off the plateau and moving over open water (Lang et al. 2007; Nesbitt et al. 2008).

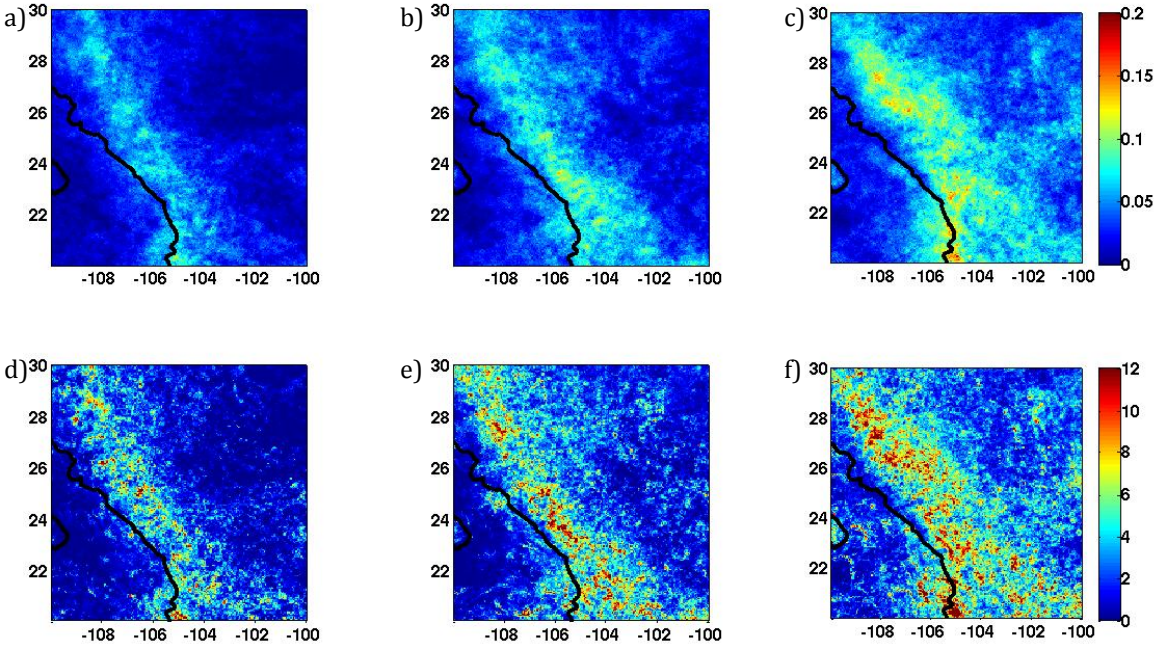

Figure 10. Sierra Madre Occidental TRMM PR 2A25v6 precipitation products for the total precipitable water subsets. Top three panels are rain frequency and bottom three panels are rain rate in mm day^{-1}. PW values range from (a,d) -0.09 – 0.01 s^{-1} (0-33%), (b,e) 0.01 – 0.04 s^{-1} (33-66%), and (c,f) 0.04 – 0.12 s^{-1} (66-100%).

3.1.5 – Western Ghats

Sounding parameters are useful in determining precipitation location, intensity, and rain rate patterns in the Western Ghats. Figure 11 shows the precipitation products for CIN. Low CIN values restrict the regions of high rain

frequencies to the peaks while high rain rates are spread over a broader area (Figs. 11a, 11d). As CIN increases, a stronger cap on the atmosphere is present, and therefore both the rain frequency and rain rate decrease over the terrain and are confined to much lower values over the coastal areas and ocean as precipitation is suppressed (Figs. 11c, 11f).

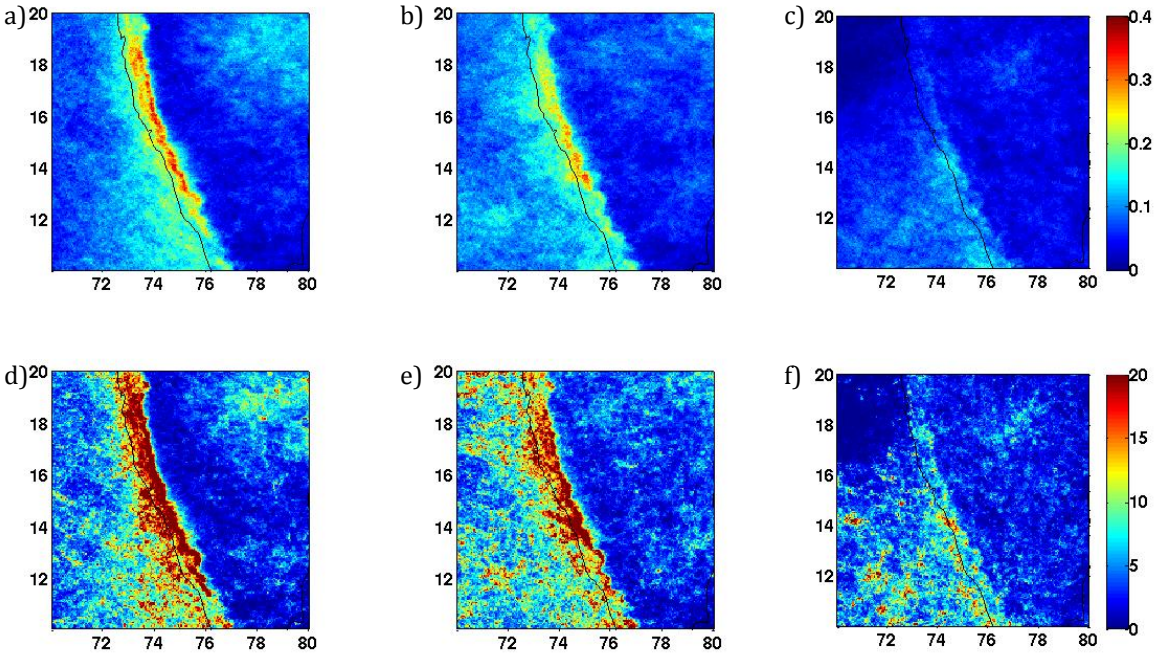

Figure 11. Western Ghats TRMM PR 2A25v6 precipitation products for the CIN subsets. Top three panels are rain frequency and bottom three panels are rain rate in mm day^{-1}. CIN values range from (a,d) 0.00 – 0.83 J kg^{-1} (0-33%), (b,e) 0.83 – 7.0 J kg^{-1} (33-66%), and (c,f) 7.0 – 258.1 J kg^{-1} (66-100%).

The moist Froude number is a key controller of precipitation frequency and rain rate in the Western Ghats. For low moist Froude numbers, rain frequency and rain rate are very low over the terrain as seen in Figures 12a and 12d. As the moist Froude number increases, precipitation frequency and intensity increase dramatically over the complex terrain as well as off shore (Figs. 12c, 12f). This

widespread increase in precipitation may be the result of decreased stability in the region.

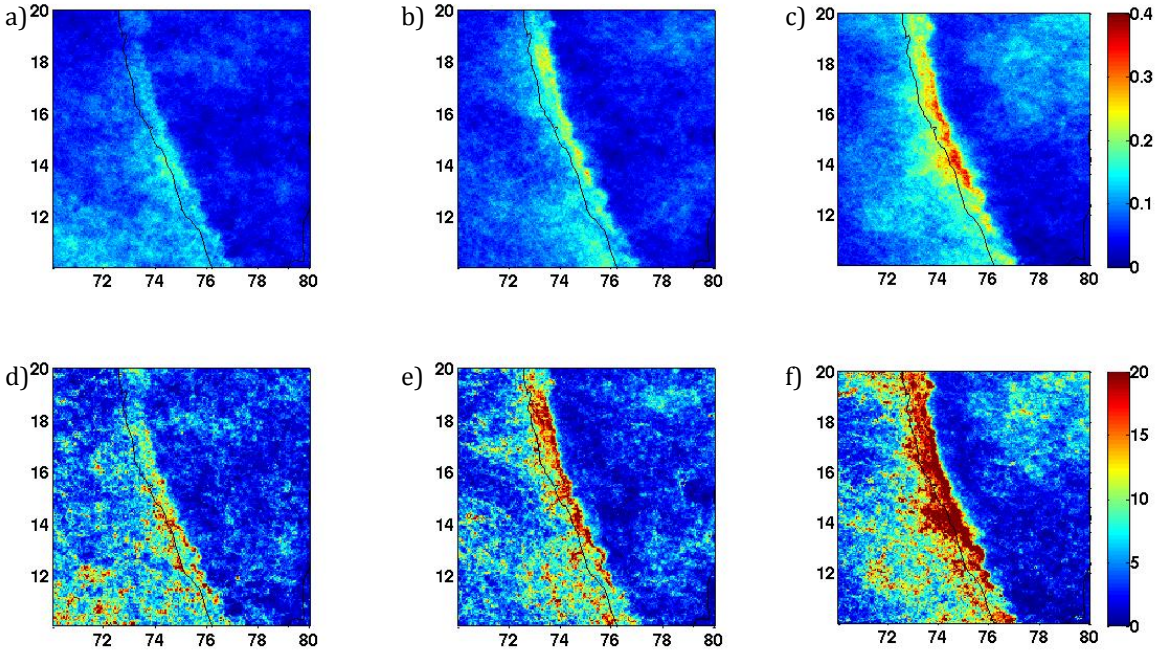

Figure 12. Western Ghats TRMM PR 2A25v6 precipitation products for the moist Froude number subsets. Top three panels are rain frequency and bottom three panels are rain rate in mm day^{-1}. F_w values range from (a,d) -0.54 – 0.19 s^{-1} (0-33%), (b,e) 0.19 – 0.30 s^{-1} (33-66%), and (c,f) 0.30 – 0.67 s^{-1} (66-100%).

3.2 – Multi-Regional Analyses

To investigate relationships between the dynamic and thermodynamic variables and parameters and the orographic precipitation impacts across all regions, multi-regional comparisons will be analyzed.

3.2.1 – Percentile Analyses

The percentile analyses focus on the average rain rate and rain frequency for select variables and parameters across all regions.

Figures 13 and 14 show the wet season average rain rate and rain frequency for the parameter CAPE sorted into twenty percentiles for each region of complex terrain. The tropical Andes, Eastern Himalayas, and Western Ghats show a slight upward trend in both rain rate and rain frequency as CAPE increases, while the Sierra Madre Occidental remains relatively constant. Hawaii displays a strong upward trend from the 50th percentile onward. The variations in the frequency and rain rate trends demonstrate the parameter CAPE should only be used for regional analyses.

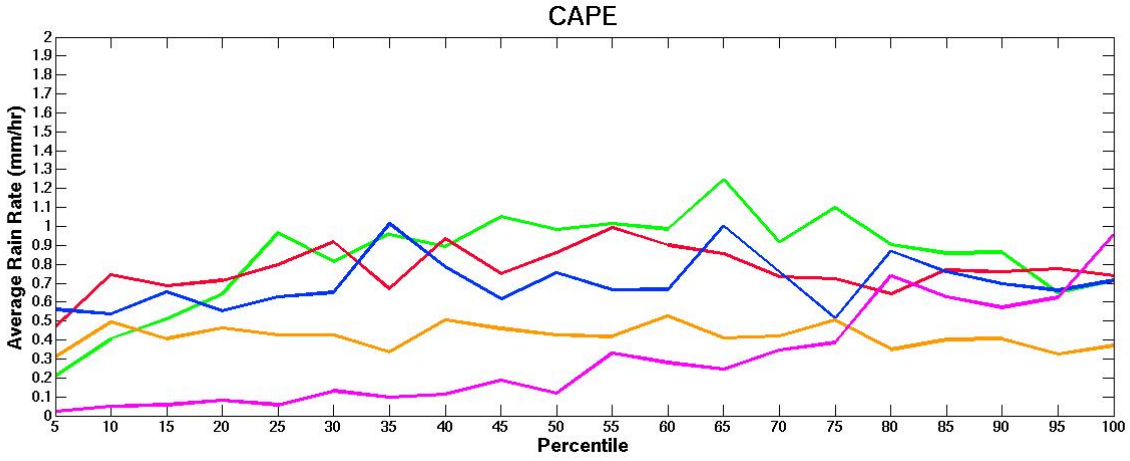

Figure 13. Multi-regional trend analysis showing how wet season average rain rate in mm day^{-1} changes based on CAPE values sorted into twenty percentiles. CAPE values increase with increasing percentiles. Line colors represent regions of interest. Blue – Tropical Andes, Pink – Hawaii, Red – Eastern Himalayas, Orange – Sierra Madre Occidental, Green – Western Ghats

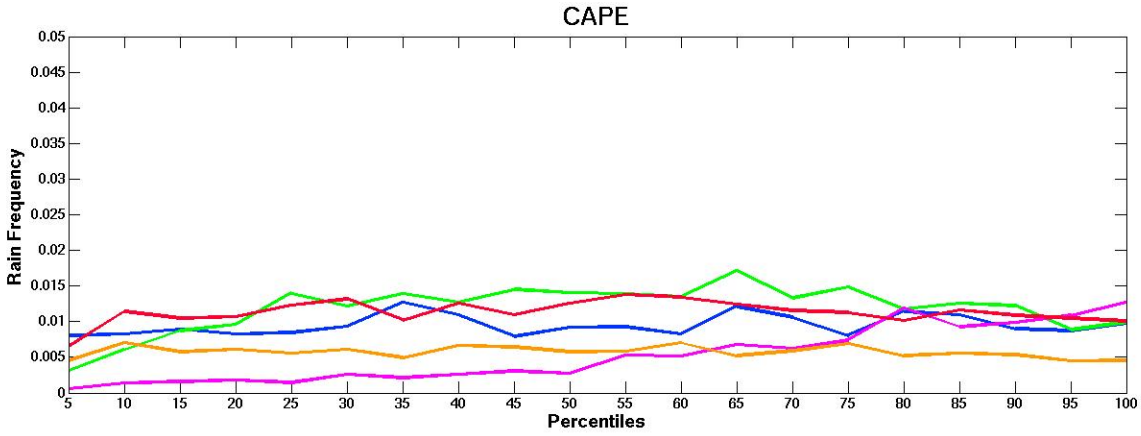

Figure 14. Multi-regional trend analysis showing how wet season rain frequency changes based on CAPE values sorted into twenty percentiles. CAPE values increase with increasing percentiles. Line colors represent regions of interest. Blue – Tropical Andes, Pink – Hawaii, Red – Eastern Himalayas, Orange – Sierra Madre Occidental, Green – Western Ghats

The wet season average rain rate and rain frequency multi-regional trends show a relatively steady decrease with increased CIN in multiple regions while others show less regionally-clear trends as seen in Figures 15 and 16. The Eastern Himalayas, Sierra Madre Occidental, and Western Ghats all show decreasing frequencies and rates with increasing CIN, while the tropical Andes remain nearly constant. Hawaii exhibits a sharp increase in rate and frequency around the 40th percentile then decreases slightly with increasing CIN. The three plateau regions demonstrate decreasing trends with increasing CIN while the other two regions do not. This may suggest that CIN impacts orographic precipitation characteristics differently based on physical terrain characteristics. A larger multi-regional study with more sample regions would be necessary to confirm this hypothesis.

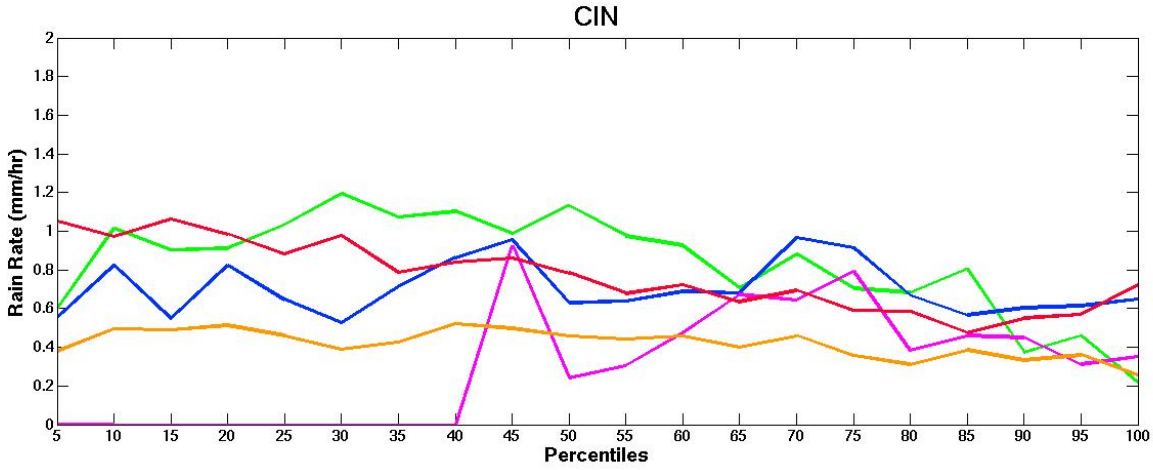

Figure 15. Multi-regional trend analysis showing how wet season average rain rate in mm day^{-1} changes based on CIN values sorted into twenty percentiles. CIN values increase with increasing percentiles. Line colors represent regions of interest. Blue – Tropical Andes, Pink – Hawaii, Red – Eastern Himalayas, Orange – Sierra Madre Occidental, Green – Western Ghats

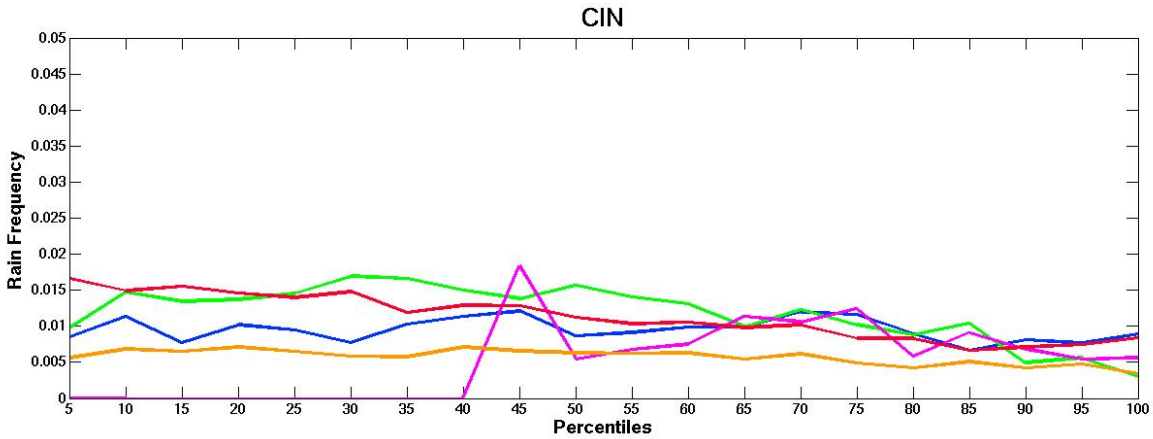

Figure 16. Multi-regional trend analysis showing how wet season rain frequency changes based on CIN values sorted into twenty percentiles. CIN values increase with increasing percentiles. Line colors represent regions of interest. Blue – Tropical Andes, Pink – Hawaii, Red – Eastern Himalayas, Orange – Sierra Madre Occidental, Green – Western Ghats

Figures 17 and 18 represent the multi-regional impacts of the LCL on rain rate and frequency. The rain rate and frequency decrease as the cloud base height increases in all regions of interest. A similar trend is seen when analyzing LFC.

Although variations in the magnitude of the trend are present, because all regions show a similar downward trend with increasing LCL and LFC heights, both the LCL and LFC have the potential to be utilized when analyzing general precipitation trends on a multi-regional scale.

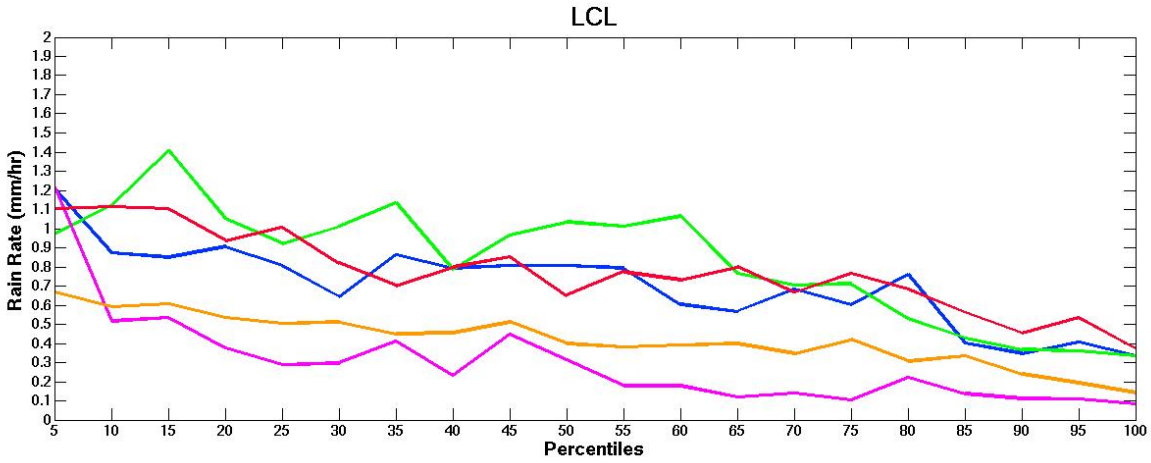

Figure 17. Multi-regional trend analysis showing how wet season average rain rate in mm day^{-1} changes based on LCL heights sorted into twenty percentiles. LCL heights increase with increasing percentiles. Line colors represent regions of interest. Blue – Tropical Andes, Pink – Hawaii, Red – Eastern Himalayas, Orange – Sierra Madre Occidental, Green – Western Ghats

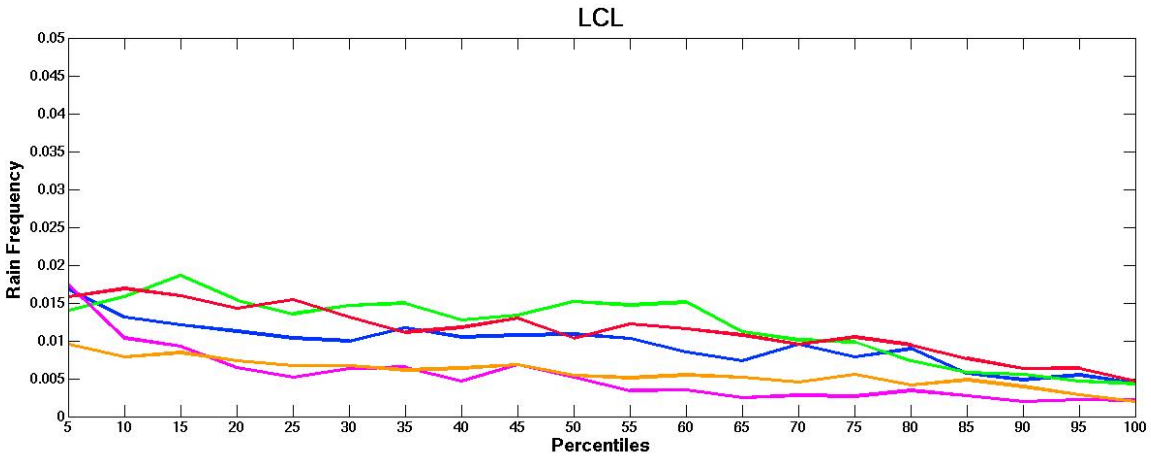

Figure 18. Multi-regional trend analysis showing how wet season rain frequency changes based on LCL heights sorted into twenty percentiles. LCL heights increase with increasing percentiles. Line colors represent regions of interest. Blue – Tropical Andes, Pink – Hawaii, Red – Eastern Himalayas, Orange – Sierra Madre Occidental, Green – Western Ghats

The mean wet season average rain rate and frequency trends for $\bar{\theta}_v$ demonstrate a mix of increasing and decreasing trends as seen in Figures 19 and 20. The tropical Andes, Eastern Himalayas, and Sierra Madre Occidental all show a decreasing trend with increasing $\bar{\theta}_v$. The Western Ghats show an initial upward trend peaking around the 40th percentile and decreasing thereafter, while Hawaii shows a slight upward trend throughout. The multiple trend directions and magnitudes suggest that $\bar{\theta}_v$ should not be used on a multi-regional scale for orographic precipitation analyses.

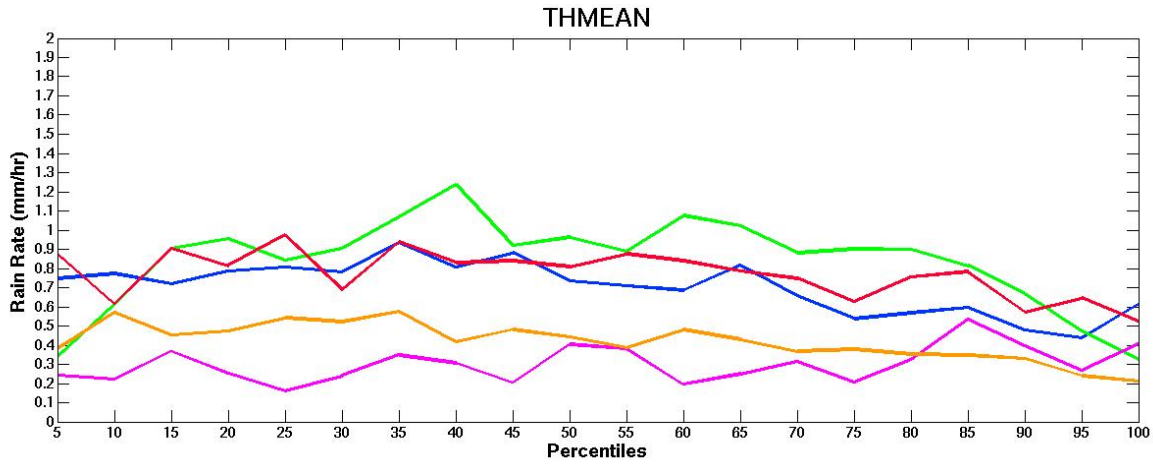

Figure 19. Multi-regional trend analysis showing how wet season average rain rate in mm day^{-1} changes based on $\overline{\theta}_v$ values sorted into twenty percentiles. $\overline{\theta}_v$ values increase with increasing percentiles. Line colors represent regions of interest. Blue – Tropical Andes, Pink – Hawaii, Red – Eastern Himalayas, Orange – Sierra Madre Occidental, Green – Western Ghats

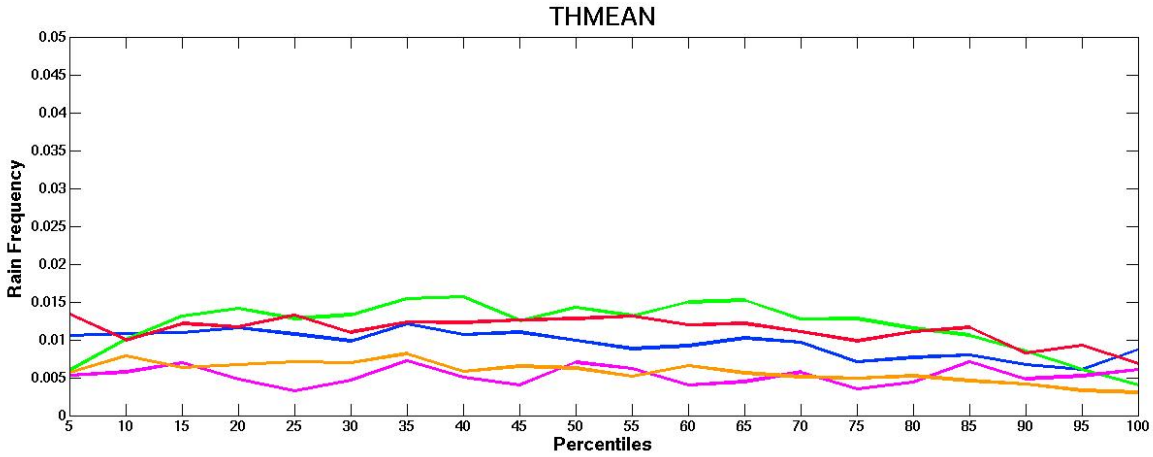

Figure 20. Multi-regional trend analysis showing how wet season rain frequency changes based on $\overline{\theta}_v$ values sorted into twenty percentiles. $\overline{\theta}_v$ values increase with increasing percentiles. Line colors represent regions of interest. Blue – Tropical Andes, Pink – Hawaii, Red – Eastern Himalayas, Orange – Sierra Madre Occidental, Green – Western Ghats

Figures 21 and 22 indicate how the wet season average rain rate and rain frequency are impacted as the lapse rate of the mean virtual potential temperature changes. Similar to the mean virtual potential temperature trends, the lapse rate

impacts each region differently. The Eastern Himalayas and Sierra Madre Occidental rates and frequencies increase with increasing lapse rates, while the tropical Andes increase slightly initially, but decrease sharply once the highest lapse rates are achieved. The Western Ghats remain relatively constant throughout, but follow a similar trend to the tropical Andes once the highest lapse rates are reached. Hawaii rain rates and frequencies decrease with increasing lapse rates. The vast variation in trends suggests that the lapse rate of the mean virtual potential temperature should not be used for multi-regional analyses of orographic precipitation.

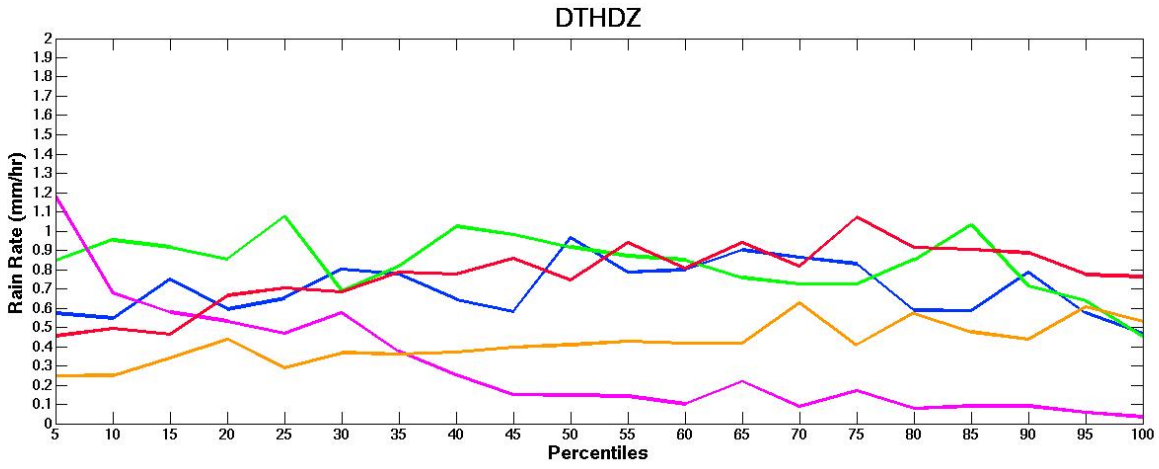

Figure 21. Multi-regional trend analysis showing how wet season average rain rate in mm day^{-1} changes based on the lapse rate of $\overline{\theta}_v$ values sorted into twenty percentiles. Lapse rate values increase with increasing percentiles. Blue – Tropical Andes, Pink – Hawaii, Red – Eastern Himalayas, Orange – Sierra Madre Occidental, Green – Western Ghats

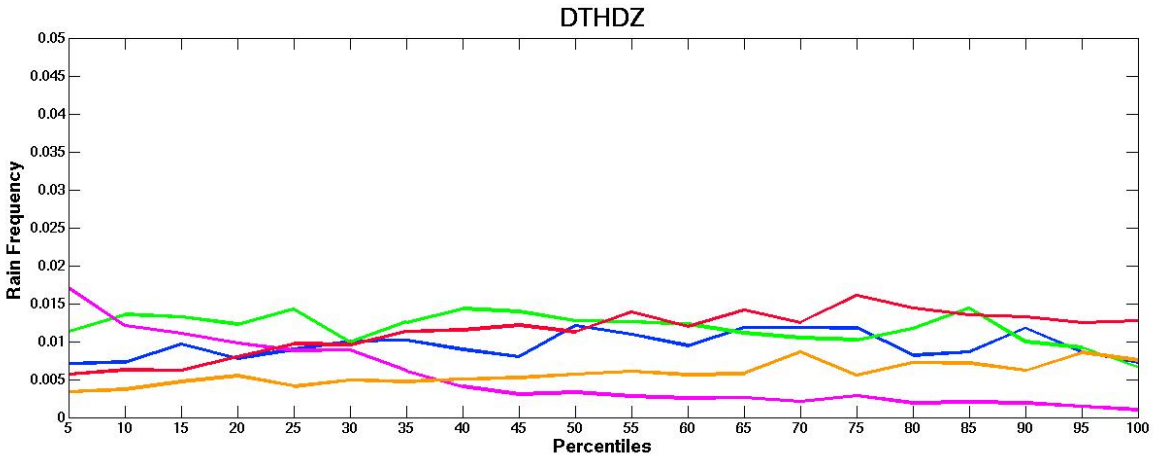

Figure 22. Multi-regional trend analysis showing how wet season rain frequency changes based on lapse rate of $\overline{\theta}_v$ values sorted into twenty percentiles. Lapse rate of $\overline{\theta}_v$ values increase with increasing percentiles. Line colors represent regions of interest. Blue – Tropical Andes, Pink – Hawaii, Red – Eastern Himalayas, Orange – Sierra Madre Occidental, Green – Western Ghats

The tropical Andes, Eastern Himalayas, and Western Ghats wet season precipitation rates and frequencies are heavily influenced by the strength of the cross-barrier flow as seen in Figures 23 and 24. As the cross-barrier flow increases, the rain rate and frequency also increase. The increasing trend is likely due to greater moisture availability leading to larger amounts of moisture being advected into the regions of complex terrain by the stronger winds as each of these regions is characterized by a sizeable area of complex terrain with a moisture source near by. Over the Sierra Madre Occidental, only a slight increase in rain rate and frequency is discernable. One hypothesis for only having the slight increase is while increased flow potentially advects more moisture over the complex terrain, the increased flow also decreases the resonance time of mesoscale convective systems over the plateau

as the faster flow leads to faster propagation speeds and lower rain rates and frequencies. The rain rate and frequency of precipitation in Hawaii is greatly impacted by cross-barrier flow. A noticeably sharp upward trend is evident as cross-barrier flow increases. The large trend deviations of rain rate and frequency for cross-barrier flow advocate that the parameter should not be used in multi-regional orographic precipitation analyses. On the contrary, the grouped trends of the tropical Andes, Eastern Himalayas, and Western Ghats suggest that cross-barrier flow may potentially be used in multi-regional analyses if the regions were subset based on characteristics of mountain range width and location relative to a moisture source. A larger study with more regions of similar and dissimilar complex terrain characteristics would be necessary to confirm this hypothesis.

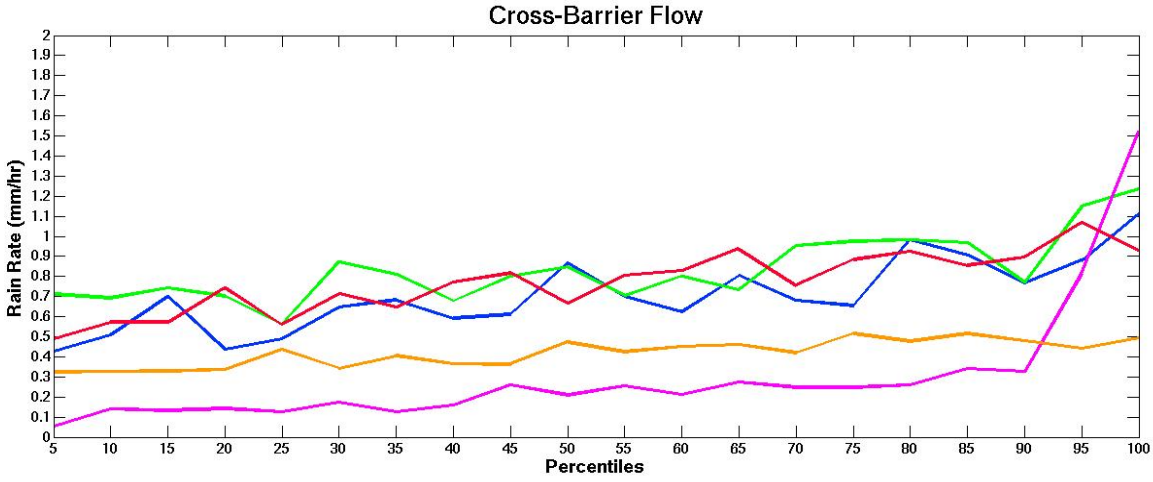

Figure 23. Multi-regional trend analysis showing how wet season average rain rate in mm day^{-1} changes based on u^* values sorted into twenty percentiles. u^* values increase with increasing percentiles. Line colors represent regions of interest. Blue – Tropical Andes, Pink – Hawaii, Red – Eastern Himalayas, Orange – Sierra Madre Occidental, Green – Western Ghats

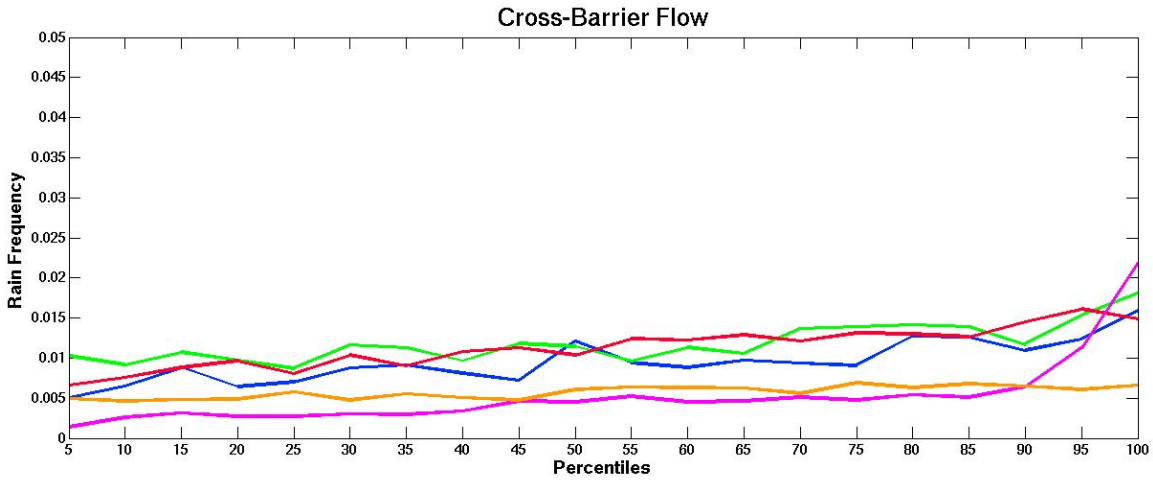

Figure 24. Multi-regional trend analysis showing how wet season rain frequency changes based on u^* values sorted into twenty percentiles. u^* values increase with increasing percentiles. Line colors represent regions of interest. Blue – Tropical Andes, Pink – Hawaii, Red – Eastern Himalayas, Orange – Sierra Madre Occidental, Green – Western Ghats

Figures 25 and 26 represent how the moist Froude number impacts the wet season average rain rate and frequency. The moist Froude number and cross-barrier flow show similar trends as the moist Froude number is partially calculated using cross-barrier flow. Evidence from this study suggests that the while all regions show an upward trend with an increasing moist Froude number, the magnitude of the trends are very different, and therefore more extensive research needs to be conducted to determine if the terrain and water source characteristics discussed in the cross-barrier flow section have the potential to make the moist Froude number a more universal orographic precipitation determinant.

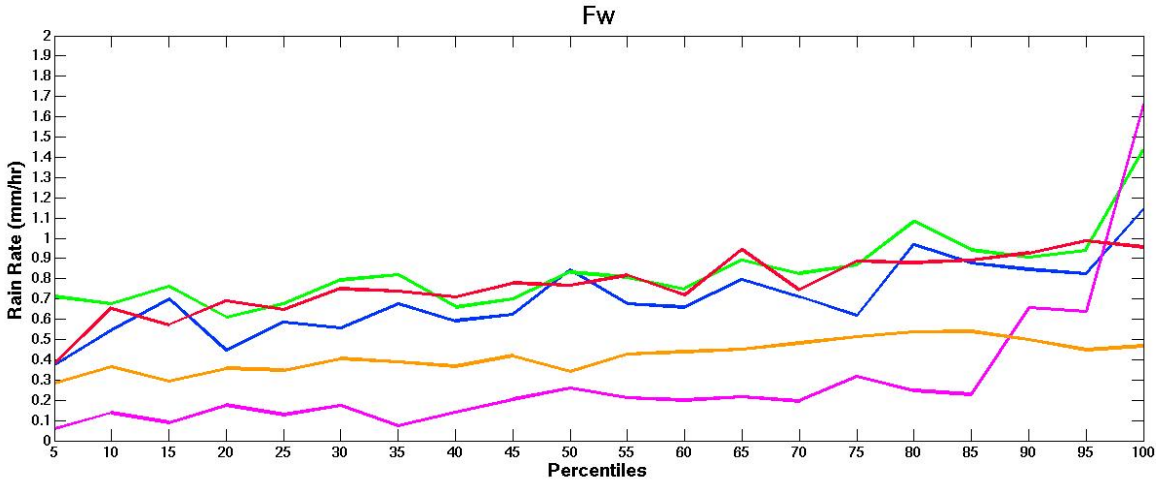

Figure 25. Multi-regional trend analysis showing how wet season average rain rate in mm day^{-1} changes based on F_w values sorted into twenty percentiles. F_w values increase with increasing percentiles. Line colors represent regions of interest. Blue – Tropical Andes, Pink – Hawaii, Red – Eastern Himalayas, Orange – Sierra Madre Occidental, Green – Western Ghats

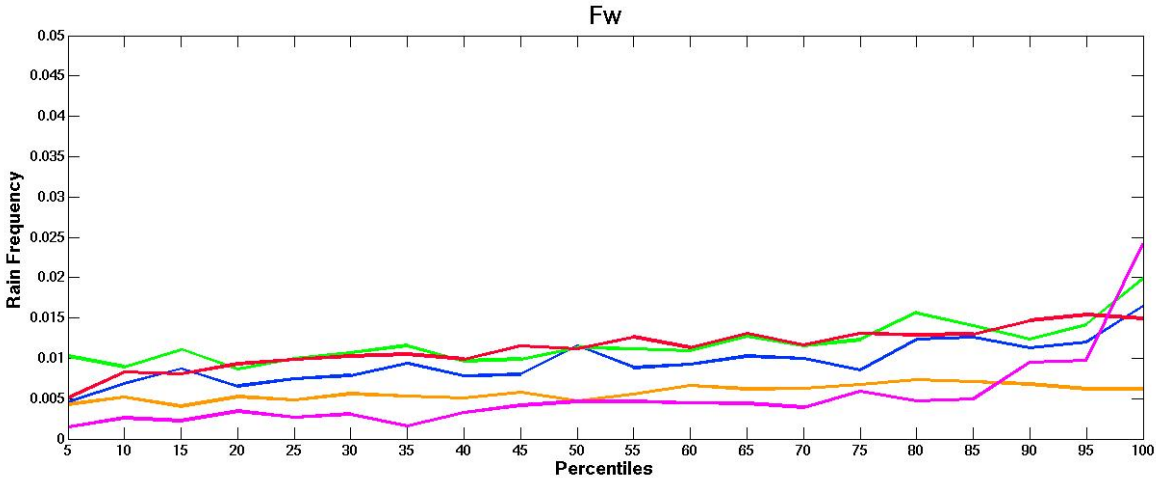

Figure 26. Multi-regional trend analysis showing how wet season rain frequency changes based on F_w values sorted into twenty percentiles. F_w values increase with increasing percentiles. Line colors represent regions of interest. Blue – Tropical Andes, Pink – Hawaii, Red – Eastern Himalayas, Orange – Sierra Madre Occidental, Green – Western Ghats

The multi-regional influences of mid-level moisture on the wet season average rain rate and frequency are shown stratified by the 700-300 hPa layer relative humidity field in Figures 27 and 28. All regions demonstrate a clear upward trend in rate and frequency as the mid-level moisture increases. A similar trend is seen in the low-level moisture analysis. The Sierra Madre Occidental shows a smaller upward trend than the other regions. The reduced trend is likely due to the lack of available moisture in the region. The similar upward trend with increasing moisture in all regions for both low and mid-level moist indicates the potential for universal applicability in orographic precipitation analyses.

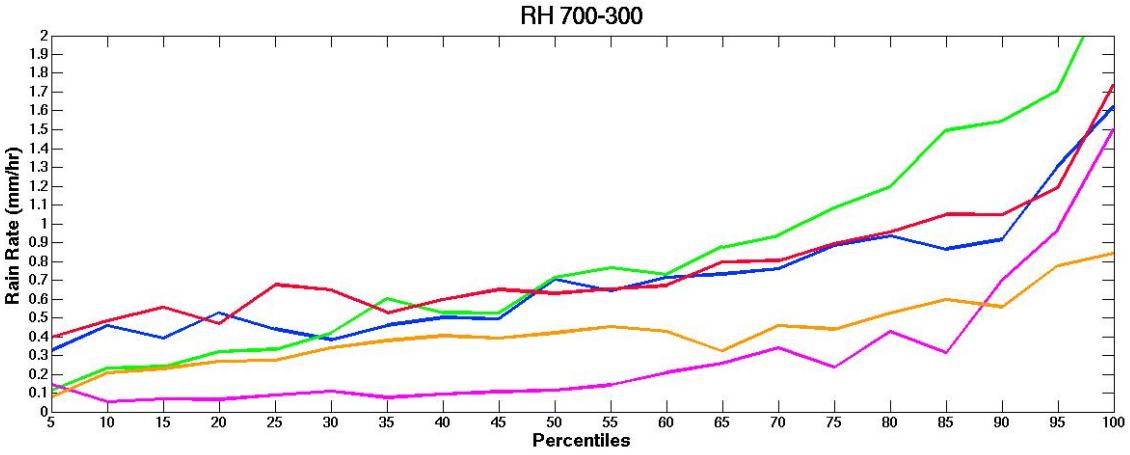

Figure 27. Multi-regional trend analysis showing how wet season average rain rate in mm day^{-1} changes based on $RH_{700\text{-}300}$ values sorted into twenty percentiles. $RH_{700\text{-}300}$ values increase with increasing percentiles. Line colors represent regions of interest. Blue – Tropical Andes, Pink – Hawaii, Red – Eastern Himalayas, Orange – Sierra Madre Occidental, Green – Western Ghats

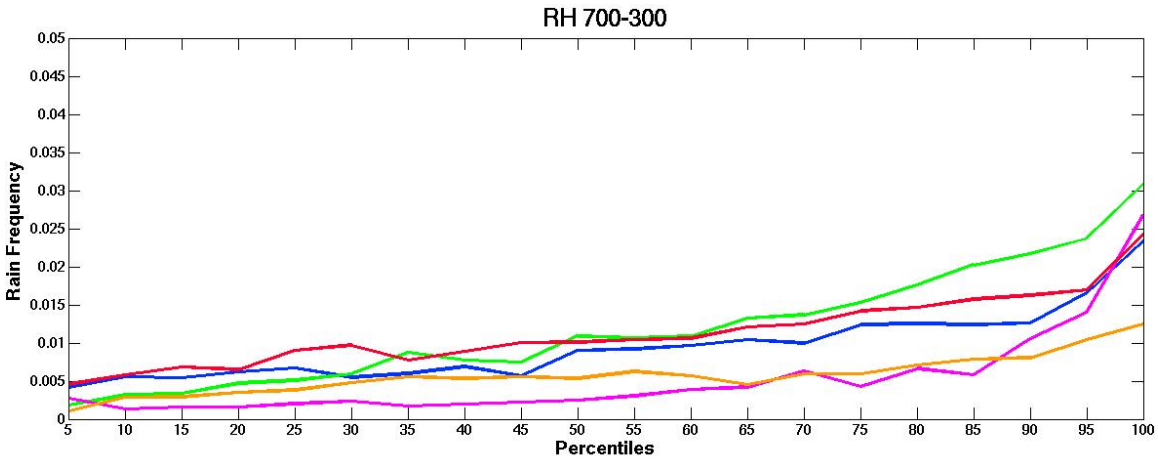

Figure 28. Multi-regional trend analysis showing how wet season rain frequency changes based on $RH_{700\text{-}300}$ values sorted into twenty percentiles. $RH_{700\text{-}300}$ values increase with increasing percentiles. Line colors represent regions of interest. Blue – Tropical Andes, Pink – Hawaii, Red – Eastern Himalayas, Orange – Sierra Madre Occidental, Green – Western Ghats

The 700 hPa specific humidity wet season average rain rate and frequency trends (Figs. 29 and 30) are very similar to the mid-level moisture trends evident in the 700-300 layer relative humidity field (Figs. 27 and 28). All regions show an upward trend in precipitation rate and frequency with the Sierra Madre Occidental showing the most gradual trend. Due to the similar nature of the precipitation characteristic trends for all regions, 700 hPa specific humidity is likely a good candidate for multi-regional analyses on orographic precipitation.

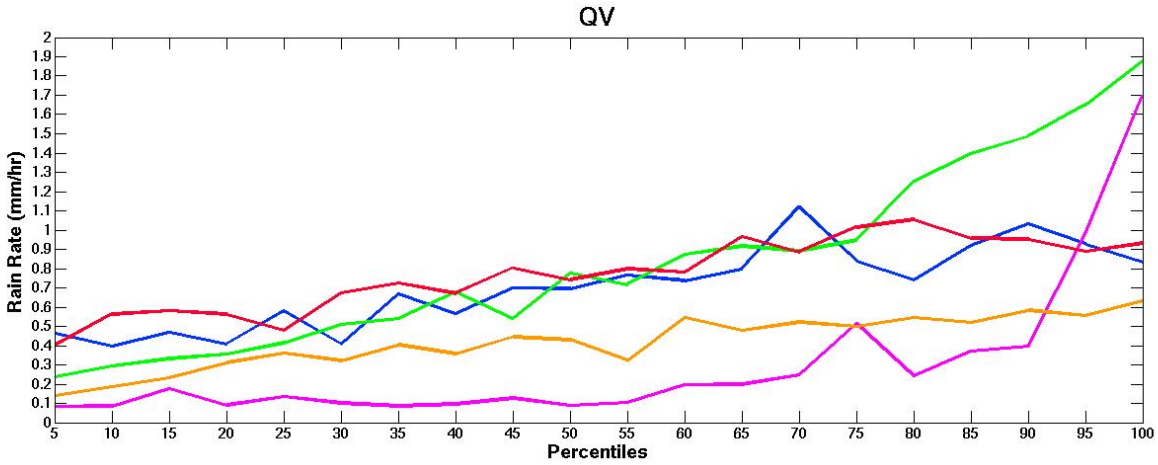

Figure 29. Multi-regional trend analysis showing how wet season average rain rate in mm day^{-1} changes based on QV_{700} values sorted into twenty percentiles. QV_{700} values increase with increasing percentiles. Line colors represent regions of interest. Blue – Tropical Andes, Pink – Hawaii, Red – Eastern Himalayas, Orange – Sierra Madre Occidental, Green – Western Ghats

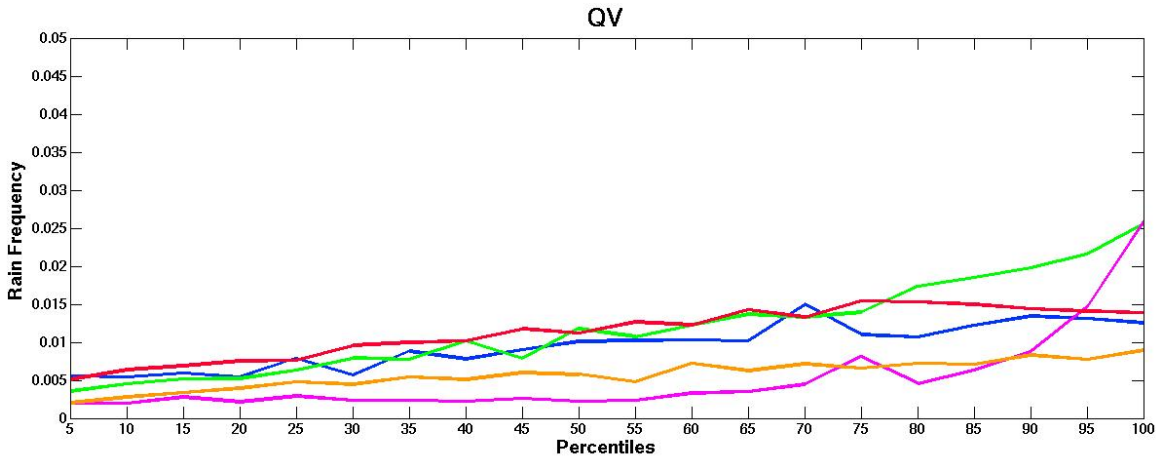

Figure 30. Multi-regional trend analysis showing how wet season rain frequency changes based on QV_{700} values sorted into twenty percentiles. QV_{700} values increase with increasing percentiles. Line colors represent regions of interest. Blue – Tropical Andes, Pink – Hawaii, Red – Eastern Himalayas, Orange – Sierra Madre Occidental, Green – Western Ghats

The final multi-regional trend analysis involves total precipitable water (Figs. 31 and 32). Unlike the other multi-regional moisture analyses, the total precipitable

water multi-regional trends are not as distinct. Rain rates and frequencies for the tropical Andes and Hawaii remain relatively constant with increased total precipitable water, while the Eastern Himalayas show a slight upward trend. The Sierra Madre Occidental and Western Ghats both display strong upward trends, with the Western Ghats trend showing the greatest increase. While some regions display the pronounced upward trends in rain rate and frequency demonstrated by other moisture variables, the combined multi-regional analysis suggest total precipitable water should not be used on a multi-regional scale to assess orographic precipitation characteristics.

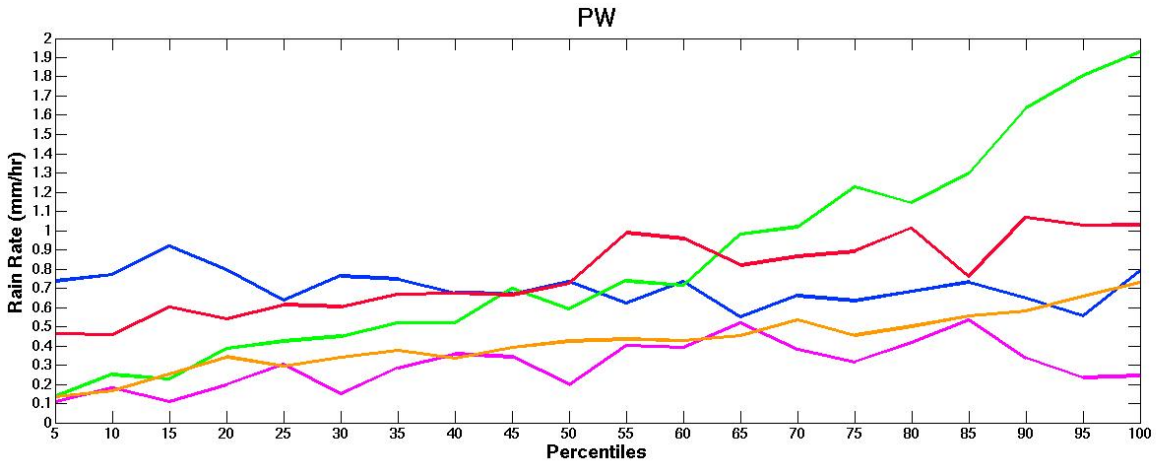

Figure 31. Multi-regional trend analysis showing how wet season average rain rate in mm day^{-1} changes based on *PW* values sorted into twenty percentiles. *PW* values increase with increasing percentiles. Line colors represent regions of interest. Blue – Tropical Andes, Pink – Hawaii, Red – Eastern Himalayas, Orange – Sierra Madre Occidental, Green – Western Ghats

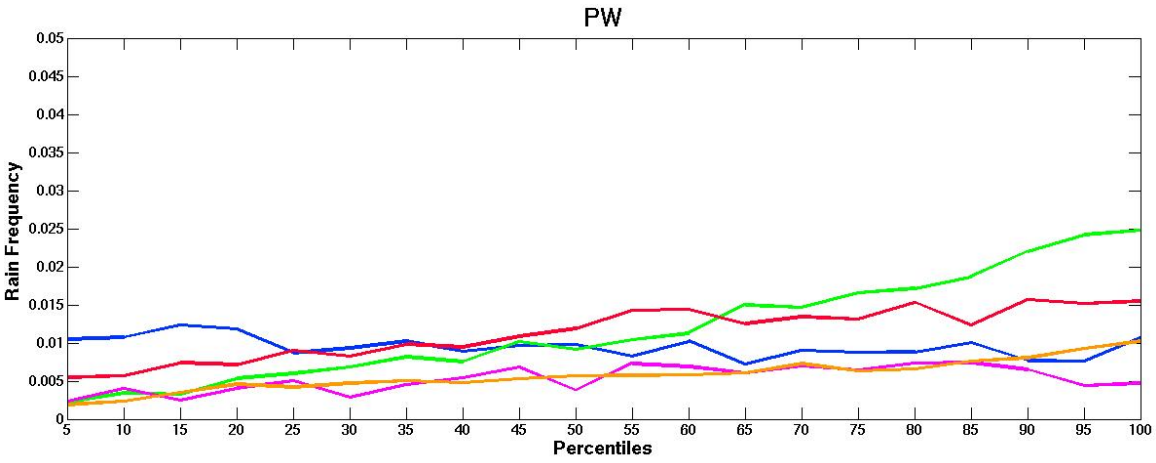

Figure 32. Multi-regional trend analysis showing how wet season rain frequency changes based on *PW* values sorted into twenty percentiles. *PW* values increase with increasing percentiles. Line colors represent regions of interest. Blue – Tropical Andes, Pink – Hawaii, Red – Eastern Himalayas, Orange – Sierra Madre Occidental, Green – Western Ghats

3.2.2 – Spatial Correlation Analysis

To further examine the conclusions drawn in the previous section, correlation coefficients between the wet season average rain rate and a couple variables and parameters are evaluated.

Based on the multi-regional analysis of the wet season average rain rate and rain frequency for the parameter CAPE, the conclusion was made that due to variations in the trends from each region, CAPE should not be used to analyze precipitation characteristics on a multi-regional scale. Figure 33 validates this hypothesis. The correlation coefficient between CAPE and rain rate is shown for each region's corresponding wet season for all twelve years of data. The figure demonstrates that the impacts of CAPE on rain rate vary significantly from region to

region. In Hawaii, CAPE and rain rate exhibit correlation coefficients between 0.8 and 1.0 near the complex terrain, while in the Sierra Madre Occidental correlation coefficients range from -0.8 to +0.8. The vast differences in correlation coefficients confirm that CAPE should only be used regionally to analyze orographic precipitation patterns and intensities.

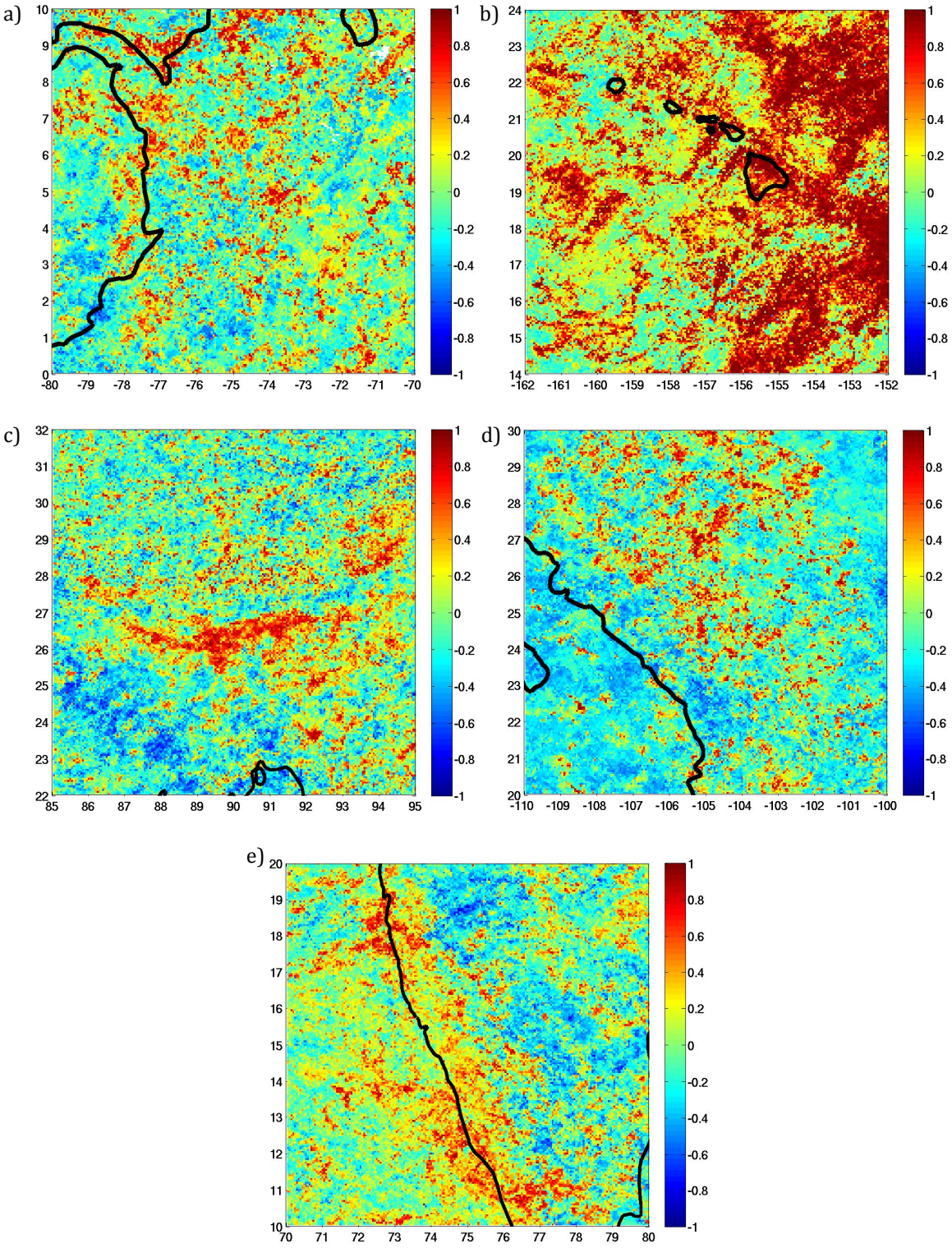

Figure 33. Multi-regional CAPE versus wet season average rain rate correlation coefficients. (a) Tropical Andes (b) Hawaii (c) Eastern Himalayas (d) Sierra Madre Occidental (e) Western Ghats

The multi-regional analyses for the low and mid-level moisture variables suggested that the 1000-700 hPa layer and 700-300 hPa layer relative humidity variables showed potential for universal applicability when conducting multi-regional analyses of tropical orographic precipitation characteristics. The multi-regional analysis coupled with the 700-300 hPa layer relative humidity and rain rate correlation coefficients strengthen the universal applicability hypothesis. Figure 34 shows that in all regions of complex terrain, the correlation coefficients are on the order of 0.8 to 1.0, and therefore mid-level moisture and rain rate are highly correlated.

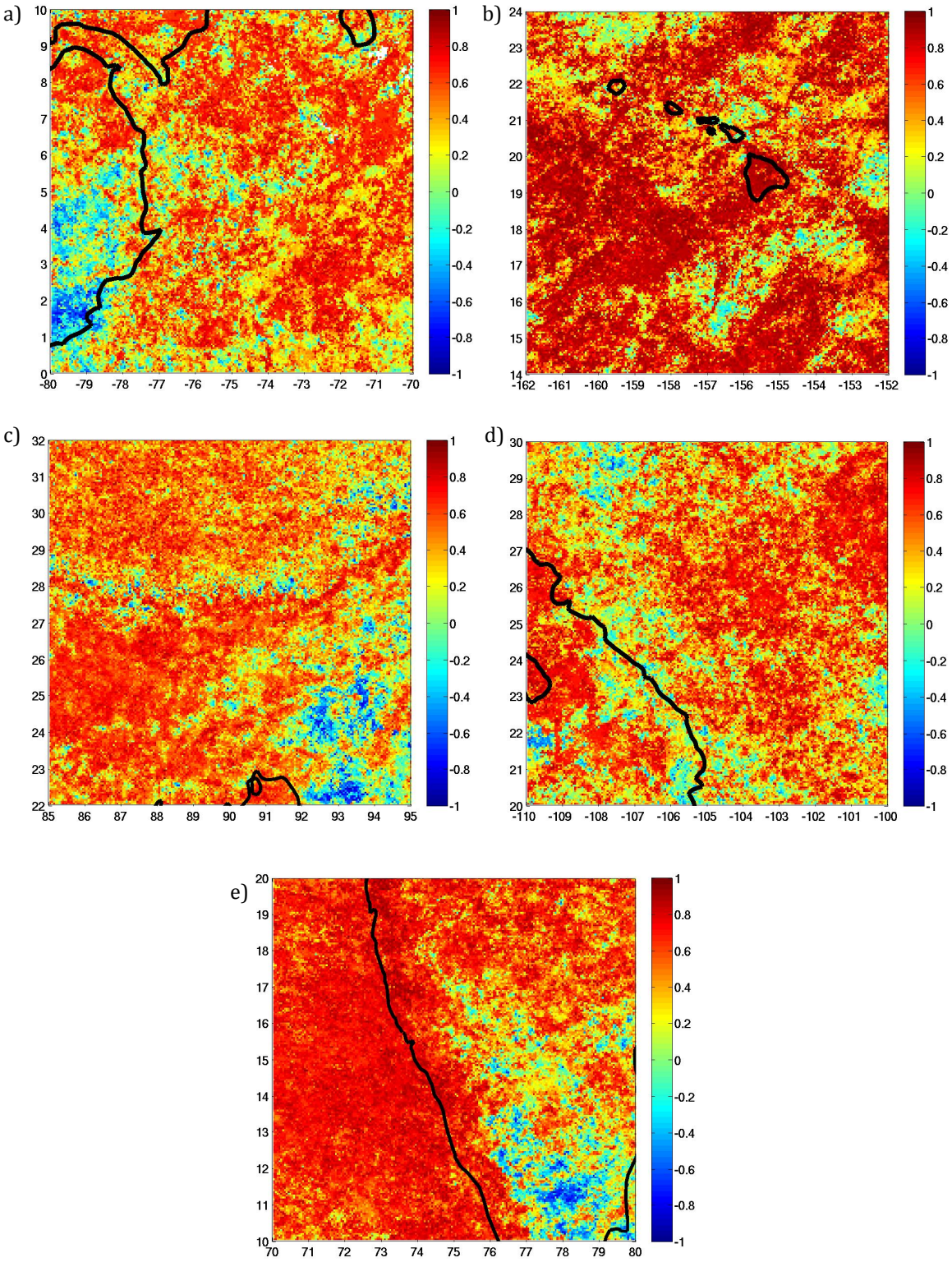

Figure 34. Multi-regional 700-300 layer relative humidity versus wet season average rain rate correlation coefficients. (a) Tropical Andes (b) Hawaii (c) Eastern Himalayas (d) Sierra Madre Occidental (e) Western Ghats

CHAPTER 4

CONCLUSIONS

TRMM PR data allows for the analysis of many new features of orographic precipitation that were not previously seen by other precipitation measuring platforms. The PR data allows for an in-depth investigation into the controlling factors of precipitation in complex terrain that otherwise may have gone unnoticed.

4.1 – Regional Conclusions

Several of the variables and parameters examined in this study have strong controls on tropical orographic precipitation. The influence on precipitation of each of the controlling factors is unique and differs substantially from region to region. Sounding and stability parameters tend to control precipitation patterns and locations while moisture variables tend to influence both frequency and intensity of the precipitation. Although these conclusions are consistent throughout multiple regions, the magnitude of the effects on precipitation characteristics of the variables and parameters are manifested differently in each region of interest.

Regional mesoscale effects may also play a key role in understanding precipitation characteristics of a particular region. Evidence of this is found in the Eastern Himalayas where a rain frequency and intensity maximum is found in the Khasi Hills near Cherrapunji. The vast amounts of precipitation that fall in this

region likely modify the surrounding atmospheric environment, and influence the orographic precipitation falling downstream over the Himalayas.

4.2 – Multi-Regional Conclusions

While multiple variables and parameters have strong controls on regional orographic precipitation, not all have the ability to be applied universally to multi-regional precipitation analyses. Moisture variables including the 1000-700 hPa and 700-300 hPa layer relative humidities and the 700 hPa specific humidity demonstrate strong multi-regional relationships with precipitation rate and frequency. Sounding parameters that incorporate moisture such as the LCL and LFC also exhibit similar relationships.

Numerous variables and parameters explain variations in orographic precipitation on a regional scale, while having little to no universal applicability. Stability parameters including the moist Froude number help to understand regional variations in precipitation, however the degree of control varies by region, and is likely dependent on local mesoscale features, and therefore should not be used on a multi-regional scale.

The tropical Andes, Eastern Himalayas, and Western Ghats all have good regional agreement of precipitation influences, while the Sierra Madre Occidental and Hawaii are often the outliers. The differences may be the result of variations in the prevailing flow not captured by our defined upstream region, or local mesoscale features such as the persistent trade-wind inversion in Hawaii or the implication

that the Gulf of California (downstream of the terrain relative to the upstream region based on prevailing 700 hPa flow used in this study) is an important moisture source for the Sierra Madre Occidental. The interactions between these synoptic and mesoscale features and the dynamic and thermodynamic variables and parameters of this study need to be evaluated to better understand the precipitation processes. More knowledge of these interactions may allow for these variables and parameters to be understood and used on a multi-regional scale.

REFERENCES

Chen, S.-H., and Y. -L. Lin, 2004: Orographic effects on a conditionally unstable flow over an idealized three-dimensional mesoscale mountain. *Meteor. Atmos. Phys.,* **88**, 1-21, doi: 0.1007/s00703-003-0047-6.

Chen, S.-H., Y. -L. Lin, 2005: Effects of moist Froude number and CAPE on a conditionally unstable flow over a mountain ridge. *J. Atmos. Sci.,* **62**, 331-350.

Emanuel, K. A., 1994: *Atmospheric Convection.* Oxford University Press, 580 pp.

Iguchi, T., T. Kozu, R. Meneghini, J. Awaka, and K. Okamoto, 2000: Rain-profiling algorithm for the TRMM precipitation radar. *J. Appl. Meteor.,* **39**, 2038-2052.

Kummerow, C., W. Barnes, T. Kozu, J. Shiue, and J. Simpson, 1998: The Tropical Rainfall Measuring Mission (TRMM) sensor package. *J. Atmos. Oceanic Tech.,* **15**, 809-817.

Lang, T. J., D. A. Ahijevych, S. W. Nesbitt, R. E. Carbone, S. A. Rutledge, and R. Cifelli, 2007: Radar-observed characteristics of precipitating systems during NAME 2004. *J. Climate,* **20**, 1713-1733.

Miglietta, M. M., and R. Rotunno, 2009: Numerical simulations of conditionally unstable flows over a mountain ridge. *J. Atmos. Sci.*, **66**, 1865-1885.

Nesbitt, S. W., D. J. Gochis, and T. J. Lang, 2008: The diurnal cycle of clouds and precipitation along the Sierra Madre Occidental observed during NAME-2004: implications for warm season precipitation estimation in complex terrain. *J. Hydrometeor,* **9**, 728-743.

Rienecker, M. M., and 28 co-authors, 2011: MERRA: NASA's Modern-Era Retrospective Analysis for Research and Applications. *J. Climate,* **24**, 3624-3648.

Shimizu, S., R. Oki, T. Tagawa, T. Iguchi, and M. Hirose, 2009: Evaluation of the effects of the orbit boost of the TRMM satellite on PR rain estimates. *J. Meteor. Soc. Japan,* **87**, 83-92.

Smolarkiewicz, P. K., R. M. Rasmussen, and T. L. Clark, 1988: On the dynamics of Hawaiian cloud bands: Island forcing. *J. Atmos. Sci.*, **45**, 1872-1905.

Yang, Y., and Y. -L. Chen, 2008: Effects of terrain heights and sizes on island-scale circulations and rainfall for the island of Hawaii during HaRP. *Mon. Wea. Rev.*, **136**, 120-146.